Stem Cell Reports
Article

ISSCR

OPEN ACCESS

Expression dynamics of HAND1/2 in *in vitro* human cardiomyocyte differentiation

Chikako Okubo,[1] Megumi Narita,[1] Azusa Inagaki,[1] Misato Nishikawa,[1] Akitsu Hotta,[2] Shinya Yamanaka,[3,4] and Yoshinori Yoshida[1,*]

[1]Department of Cell Growth and Differentiation, Center for iPS Cell Research and Application (CiRA), Kyoto University, Kyoto 606-8507, Japan
[2]Department of Clinical Application, Center for iPS Cell Research and Application (CiRA), Kyoto University, Kyoto 606-8507, Japan
[3]Department of Life Science Frontiers, Center for iPS Cell Research and Application (CiRA), Kyoto University, Kyoto 606-8507, Japan
[4]Gladstone Institute of Cardiovascular Disease, Gladstone Institutes, San Francisco, CA 94158, USA
*Correspondence: yoshinor@cira.kyoto-u.ac.jp
https://doi.org/10.1016/j.stemcr.2021.06.014

SUMMARY

Hand1 and *Hand2* are transcriptional factors, and knockout mice of these genes show left and right ventricular hypoplasia, respectively. However, their function and expression in human cardiogenesis are not well studied. To delineate their expressions and assess their functions in human cardiomyocytes (CMs) *in vitro*, we established two triple-reporter human induced pluripotent stem cell lines that express *HAND1*^{mCherry}, *HAND2*^{EGFP} and either *MYH6*-driven iRFP670 or tagBFP constitutively and investigated their expression dynamics during cardiac differentiation. On day 5 of the differentiation, *HAND1* expression marked cardiac progenitor cells. We profiled the CM subpopulations on day 20 with RNA sequencing and found that mCherry+ CMs showed higher proliferative ability than mCherry− CMs and identified a gene network of *LEF1*, *HAND1*, and *HAND2* to regulate proliferation in CMs. Finally, we identified CD105 as a surface marker of highly proliferative CMs.

INTRODUCTION

The heart structure is initiated when lateral plate mesoderm (LPM) differentiates into cardiovascular progenitor cells (CPCs) and cardiomyocytes (CMs) (Garry and Olson, 2006; Wu et al., 2008). CPCs originate from two populations in the cardiac crescent, the first and second heart field (FHF and SHF, respectively), which mainly contribute to the left ventricle (LV) and the right ventricle (RV), atria, and outflow tract (OFT), respectively (Cai et al., 2003; Meilhac and Buckingham, 2018). Nevertheless, little is known about the mechanism that forms the heart structure during cardiogenesis.

Hand1 and *Hand2* are related basic-helix-loop-helix transcriptional factors (TFs) and required for the morphological development of the heart in mice (Cserjesi et al., 1995; George and Firulli, 2019; Srivastava et al., 1995). Consistently, knockout of these genes causes severe hypoplasia of the heart dose dependently (McFadden et al., 2005). *Hand1* and *Hand2* are first expressed in LPM and cardiac crescent in mice (Cserjesi et al., 1995; de Soysa et al., 2019; Srivastava et al., 1997). From the heart tube stage, the expression of *Hand1* is restricted to the LV and OFT regions in heart development (Barnes et al., 2010; de Soysa et al., 2019; Firulli et al., 1998; McFadden et al., 2005; Meilhac and Buckingham, 2018). *Hand1* knockout is embryonic lethal in mice due to extraembryonic defects (Firulli et al., 1998; Riley et al., 1998), and mice with conditional deletions of *Hand1* demonstrated defects in looping, poorly organized ventricular septa, and LV hypoplasia and died within 3 days after birth (McFadden et al., 2005). On the other hand, mice with overexpressed *Hand1* showed disrupted heart morphogenesis with an elevated proliferation of cells and failed expansion of the LV *in vivo* (Risebro et al., 2006; Togi et al., 2004). By contrast, *Hand2* knockout mice showed hypoplasia of the RV, a thinner myocardium in the ventricle, and embryonic lethality, suggesting that *Hand2* is essential for SHF cells (Srivastava et al., 1997; Tsuchihashi et al., 2011). Recent single-cell RNA sequencing (RNA-seq) analysis showed that *Hand2*-deficient mice could give rise to RV cells but not OFT cells (de Soysa et al., 2019). These studies have suggested that *Hand1* and *Hand2* play critical roles from LPM to heart organogenesis, but the regulations and functions are hidden by the spatiotemporal complexity and heterogeneity of the heart. Additionally, the expression dynamics and functions of *HAND1* and *HAND2* in human cardiogenesis have hardly been investigated.

In humans, mutant *HAND1* causes hypoplastic left heart syndrome, suggesting human *HAND1* has a similar role to *Hand1* (Reamon-Buettner et al., 2008, 2009). A single-cell RNA-seq study of human embryonic heart reported that the expression of *HAND1* was enriched in ventricular CMs, especially in the LV at the early stage (5 weeks of gestation) (Cui et al., 2019). The same study also found that the expression of *HAND2* was widely spread but higher in atrial CMs than in ventricular CMs. Although understanding the mechanism of human heart development is beneficial for the future development of cardiac regenerative medicine, detailed analysis of human cardiogenesis has been difficult

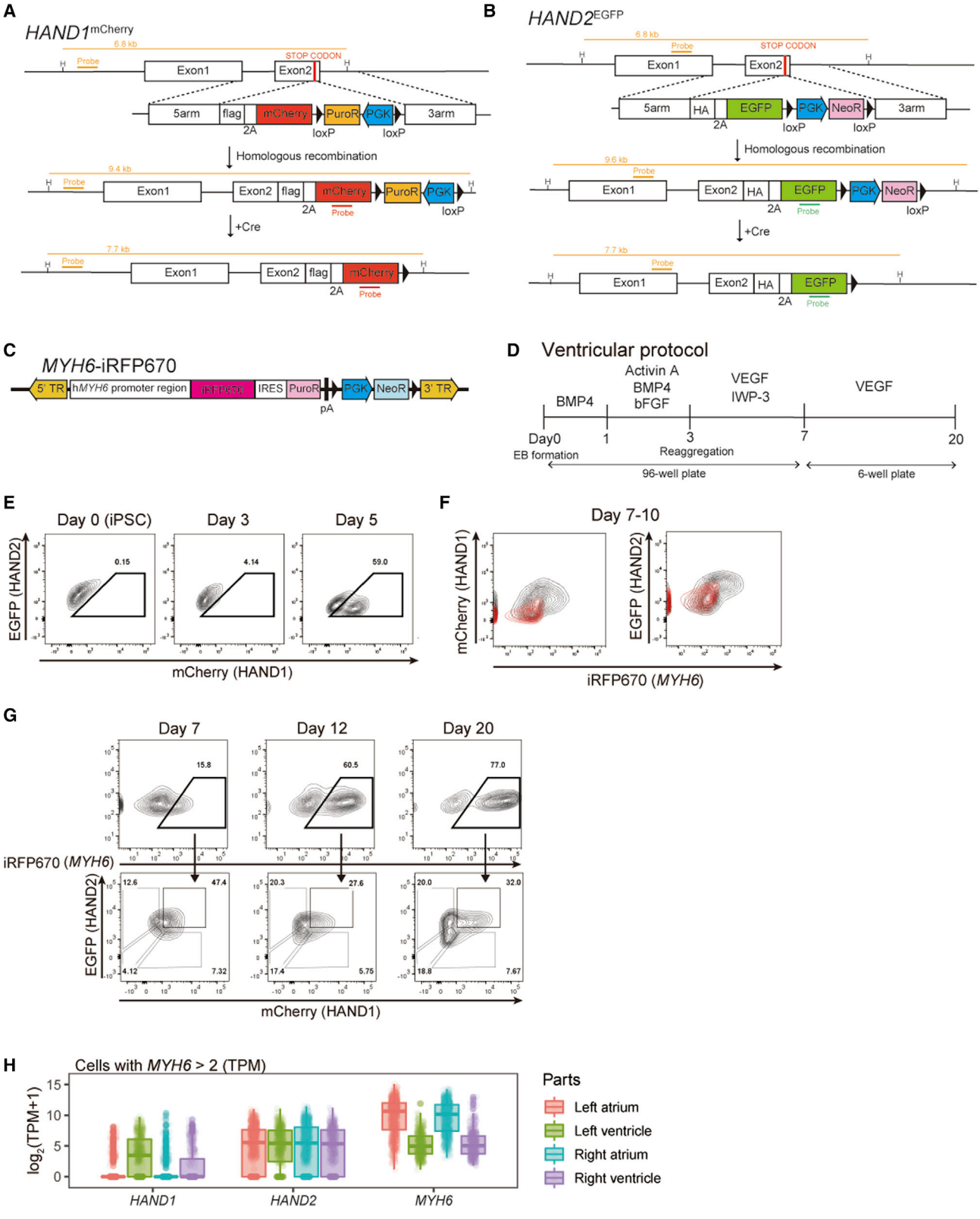

(legend on next page)

due to the limited availability of human cell sources. Human induced pluripotent stem cells (hiPSCs) recapitulate many features of cardiac lineage specification, making them an attractive model *in vitro* to study human developmental mechanisms and different CM subpopulations (Burridge et al., 2012; Protze et al., 2019; Randolph and Lian, 2019).

In the present study, to investigate the expression dynamics and molecular functions of *HAND1* and *HAND2* in human *in vitro* CM differentiation, we established *HAND1/HAND2* double-reporter hiPSCs to observe the expression dynamics and identify subpopulations during the cardiac differentiation process. By combining a third reporter fluorescent protein to mark *MYH6*-positive cardiac cells, we characterized HAND1+ and HAND1− subpopulations in the early stage and identified a new surface marker and gene regulatory network of proliferative CMs in the later stage.

RESULTS

Establishing the *HAND1*^{mCherry}, *HAND2*^{EGFP}, and *MYH6*-iRFP670 triple-reporter hiPSC line

To delineate the expression of *HAND1* and *HAND2* noninvasively and to assess their functions in differentiating human CMs *in vitro*, we established *HAND1*^{mCherry}, *HAND2*^{EGFP}, and *MYH6*-iRFP670 triple-reporter hiPSCs. We targeted an allele of the *HAND1* gene on chromosome 5 using the CRISPR-Cas9 system to insert mCherry and 2A self-cleaving peptide in front of the stop codon. Simultaneously, we introduced a single copy of the EGFP gene into the *HAND2* gene on chromosome 4 to generate double-reporter *HAND1*^{mCherry}, *HAND2*^{EGFP} hiPSCs (Figures 1A and 1B and S1A–S1E) (Mali et al., 2013). In addition, we used the *piggyBac* vector system to induce a near-infrared fluorescent protein, iRFP670, under the control of the *MYH6* promoter activity to monitor CMs to this double-reporter hiPSC line (Figures 1C, S1F, and S1G) (Funakoshi et al., 2016; Woltjen et al., 2009). This triple-reporter line was differentiated into CMs using the modified embryonic body (EB)-based protocol (Funakoshi et al., 2016; Yang et al., 2008) (Figure 1D). We observed the expression dynamics of these fluorescent proteins during differentiation by fluorescence-activated cell sorting (FACS) from day 1 of the differentiation to day 20 (Figures S2A–S2C). *HAND1*^{mCherry} was first detected from day 3, and mCherry+ and mCherry− populations were observed from day 5 (Figures 1E and S2D). Later, EGFP expression began, and iRFP670+ CMs were induced from the EGFP and mCherry high population on day 7 (Figures 1, S2D, and S2E). On day 20, four subpopulations (mCherry− EGFP−, mCherry− EGFP+, mCherry+ EGFP−, and mCherry+ EGFP+) were observed in iRFP670+ CMs, although the signal for mCherry+ EGFP− CMs was low (Figures 1G and S2E) compared with widely expressed EGFP, but mCherry was localized (Figure S2E). An analysis of single-cell RNA-seq data of human developmental heart revealed that cells highly expressing *HAND1* were enriched in the LV, but most cells expressed *HAND2* (Figure 1H) (Cui et al., 2019). These findings suggested that the different expressions of *HAND1* and *HAND2* in our *in vitro* model reflect their expressions in the developing heart.

HAND1 expression marks CPCs in the early stage *in vitro*

We investigated the mCherry+ and mCherry− populations on day 5 separately. mCherry+ cells showed higher expression levels of cardiac genes for FHF (*NKX2-5*, *TBX5*, *TBX20*, and *HCN4*) and SHF (*TBX1*, *ISL1*, *FGF10*, and *FGF8*) than mCherry− cells with one exception, *HCN4* (Figure 2A) (Andersen et al., 2018; Bruneau et al., 1999; Cai et al., 2003; Meilhac and Buckingham, 2018; Singh et al., 2005). In addition, the expressions of two CPC markers, PDGFRA and CD13, were consistent with the expression of mCherry. C-KIT, a surface marker of the earliest hematopoietic and vascular progenitors, was expressed in mCherry− cells (Figure 2B) (Kattman et al., 2011; Skelton et al.,

Figure 1. *HAND1*^{mCherry}, *HAND2*^{EGFP}, and *MYH6*-iRFP670 triple-reporter hiPSC line

(A and B) Scheme of the establishment of the *HAND1* and *HAND2* double-reporter line with mCherry and EGFP, respectively, using the CRISPR-Cas9 system and removal of the selection cassettes using the Cre/*loxP* system. 5arm, 5′ homologous arm; 3arm, 3′ homologous arm; 2A, 2A peptide; HA, HA-tag; flag, FLAG tag; PGK, promoter sequence of phosphoglycerate-kinase 1; PuroR, puromycin resistance gene; NeoR, neomycin resistance gene. HindIII (H) was used to digest genomic DNA for Southern blotting. Orange lines indicate external and internal probes for Southern blotting with expected band sizes.

(C) Construction of the *MYH6*-iRFP670 reporter with the *piggyBac* transposon system.

(D) Scheme of the ventricular CM differentiation protocol.

(E) Representative FACS plots of the expression dynamics of mCherry and EGFP on days 0, 3, and 5.

(F) Representative FACS plots of the expressions of mCherry and EGFP with iRFP670 of the triple reporter (black) and parental 409B2 (red) on day 7 of the differentiation.

(G) Representative FACS plots of subpopulations based on the expressions of mCherry and EGFP in iRFP670+ CMs on days 7, 12, and 20.

(H) Box plots of the expressions of *HAND1*, *HAND2*, and *MYH6* in LV, RV, left atrium, right atrium of the developing heart. Cells that showed *MYH6* > 2 were used for the single-cell RNA-seq data in GSE106118.

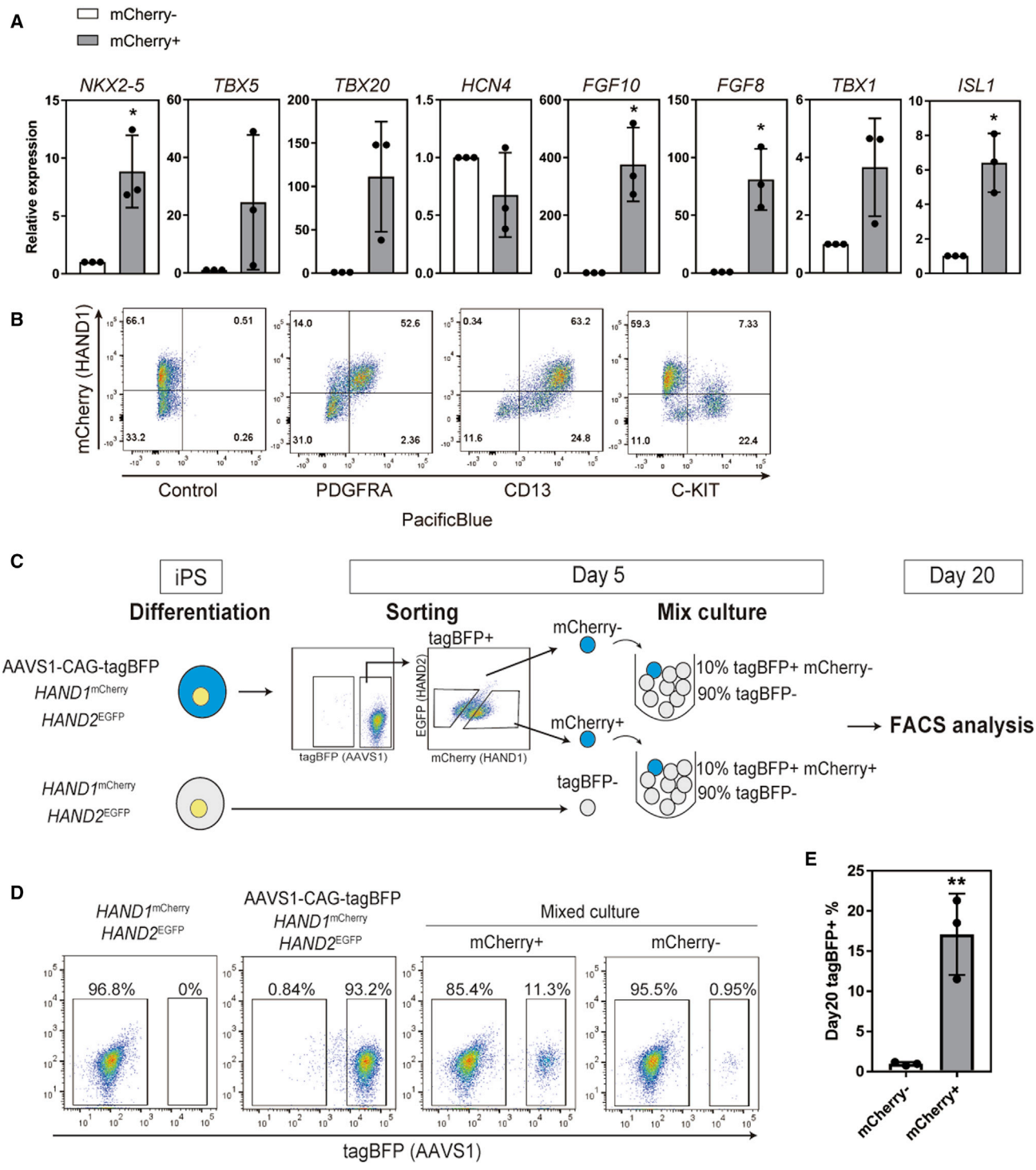

Figure 2. HAND1+ cells on day 5 contribute to the CPC population

(A) Gene expressions of the cardiac TFs *NKX2-5*, *TBX5*, *TBX20*, *HCN4*, *FGF10*, *FGF8*, *TBX1*, and *ISL1* in mCherry+ cells relative to mCherry− cells isolated on day 5 (n = 3 independent experiments). *p < 0.05 by Welch's t test.

(B) Representative FACS plots of mCherry expression with antibodies for PDGFRA, CD13, and C-KIT on day 5.

(C) Scheme of the mixed coculture system for tracing mCherry+ and mCherry− cells in EBs. To label the cells, CAG promoter-driven tagBFP was knocked into the AAVS1 locus of *HAND1*^{mCherry} *HAND2*^{EGFP} double-reporter hiPSCs (AAVS1-CAG-tagBFP). The tagBFP-labeled (tagBFP+)

(legend continued on next page)

2016; Yang et al., 2008). These results suggest that mCherry+ cells on day 5 are CPCs.

To determine if mCherry− cells had cardiac lineage fate potential, we tried to culture day 5 mCherry+ and mCherry− cell populations; however, isolated mCherry− cells did not reaggregate or reproduce EBs. Therefore, we established a mixed coculture system to trace mCherry− cells on day 5 by labeling the *HAND1*^{mCherry} and *HAND2*^{EGFP} double-reporter cell line with constitutively expressing tagBFP (Figures 2C and S3). tagBFP-labeled and non-labeled double-reporter iPSCs were differentiated into CMs simultaneously (Figure 2C). On day 5, mCherry+ and mCherry− cells were isolated from the tagBFP+ population. We then mixed the isolated tagBFP-labeled mCherry+ and mCherry− cells separately with the non-labeled parental double-reporter cells (tagBFP−) at a 1:9 ratio and continued the differentiation process until day 20. On day 20, the percentage of tagBFP+ cells in the mixed cocultures was analyzed by FACS. The percentage of tagBFP+ mCherry+ cells in the mixed culture was over 10%, but the percentage of tagBFP+ mCherry− cells was less than 2% (Figures 2D and 2E). These results indicate that mCherry− cells did not differentiate into cardiac cells after day 5. Taken together, the expression of *HAND1* at the early stage marks CPCs derived from hiPSCs.

HAND1 is upregulated by BMP4 at the early and late stages

To examine the regulation of *HAND1* and *HAND2* expressions, we manipulated the concentrations of cytokines in the differentiation protocol. For the early stage, we manipulated Activin A, bone morphogenetic protein 4 (BMP4), and basic fibroblast growth factor (bFGF) in day 0 and day 1 media and analyzed the percentages of mCherry+ cells on day 5 and iRFP670+ CMs on day 20 (Figures 3A, S4A, and S4B). BMP4 induced mCherry+ cells, but neither Activin A nor bFGF did (Figure 3B). Increasing the Activin A concentration led to fewer mCherry+ and iRFP670+ cells, but 0 ng/mL Activin A generated mCherry+ cells and no iRFP670+ CMs (Figure 3C). In contrast, increasing the BMP4 concentration promoted the number of mCherry+ and iRFP670+ cells (Figure 3D). Finally, increasing the bFGF concentration had no significant effect on the number of mCherry+ or iRFP670+ cells (Figure 3E). In these conditions, we did not observe differences in the distributions of *HAND1* and *HAND2* of day 20 CMs. These results indicate that the expression of *HAND1* at the early stage is upregulated by BMP4 and downregulated by Activin A. In addition, they suggest that the expression of *HAND1* is necessary but not sufficient to specify hiPSCs into CPCs.

We also manipulated the concentrations of vascular endothelial growth factor (VEGF) and IWP-3, a WNT signal inhibitor, in day 3 medium and VEGF and bFGF in maintenance medium after day 7 (Figures S4F and S4G). No effects were found on the mCherry expression on day 5 or the subpopulation distribution on day 20.

To further investigate the role of the signals induced by cytokines, we used several chemical inhibitors of cytokine signals, including SB431542 (TGFβ signal inhibitor), IWP-3, dorsomorphin (BMP signal inhibitor), and BMS 493 (retinoic acid [RA] signal inhibitor), from day 7 until day 20 in the cardiac differentiation (Figure 3F). The expression of mCherry decreased with the administration of IWP-3 and especially with dorsomorphin (Figures 3G–3J and S4H–S4K). Therefore, *HAND1* is regulated by the BMP signal at the early stage and late stage. In contrast, we did not find a regulator for *HAND2* expression.

Expressions of *HAND1* and *HAND2* are down- and upregulated in the atrial induction protocol, respectively

HAND2 is expressed widely in the developing heart of both species, but it is especially high in human atrial CMs (Cui et al., 2019). Mouse atrial CMs are generated from the SHF by RA signaling *in vivo* (de Soysa et al., 2019; Hochgreb et al., 2003; Rochais et al., 2009). Some studies have reported that human atrial CMs are generated from human pluripotent stem cells by RA *in vitro* (Devalla et al., 2015; Lee et al., 2017). Since CMs induced with our protocol are mainly ventricular CMs (Takaki et al., 2020), to promote atrial CM differentiation, we administered RA to the triple-reporter hiPSCs on day 3 (Figure 4A). In this differentiation condition, the relationship between *HAND2* and SHF during human *in vitro* cardiogenesis was investigated. The addition of 0.5 μM RA resulted in more EGFP+ cells and fewer mCherry+ cells in association with the upregulation of *NR2F2*, an atrial marker gene, on day 7 (Figures 4B–4D). On day 20, the majority of iRFP670+ CMs induced by RA addition was mCherry− EGFP+ (Figures 4E, S5A, and S5B). The results showed that *HAND1* and *HAND2* are down- and upregulated by RA, respectively, in atrial CM differentiation. We also confirmed the expression of *HAND1* on day 5 of the atrial protocol marks CPCs using the coculture tracing system shown in Figure 2C:

mCherry− and mCherry+ cells were isolated and mixed with non-labeled parental double-reporter cells (tagBFP−) on day 5. On day 20, the mixed cultures were analyzed by FACS.

(D) Representative FACS plots of the tagBFP expression on day 20.

(E) Percentages of tagBFP+ cells on day 20 in EBs mixed with tagBFP+ mCherry+ cells and tagBFP− cells or with tagBFP+ mCherry− cells and tagBFP− cells on day 5 (n = 3 independent experiments). **p < 0.01 by unpaired t test. Data represent means ± SD.

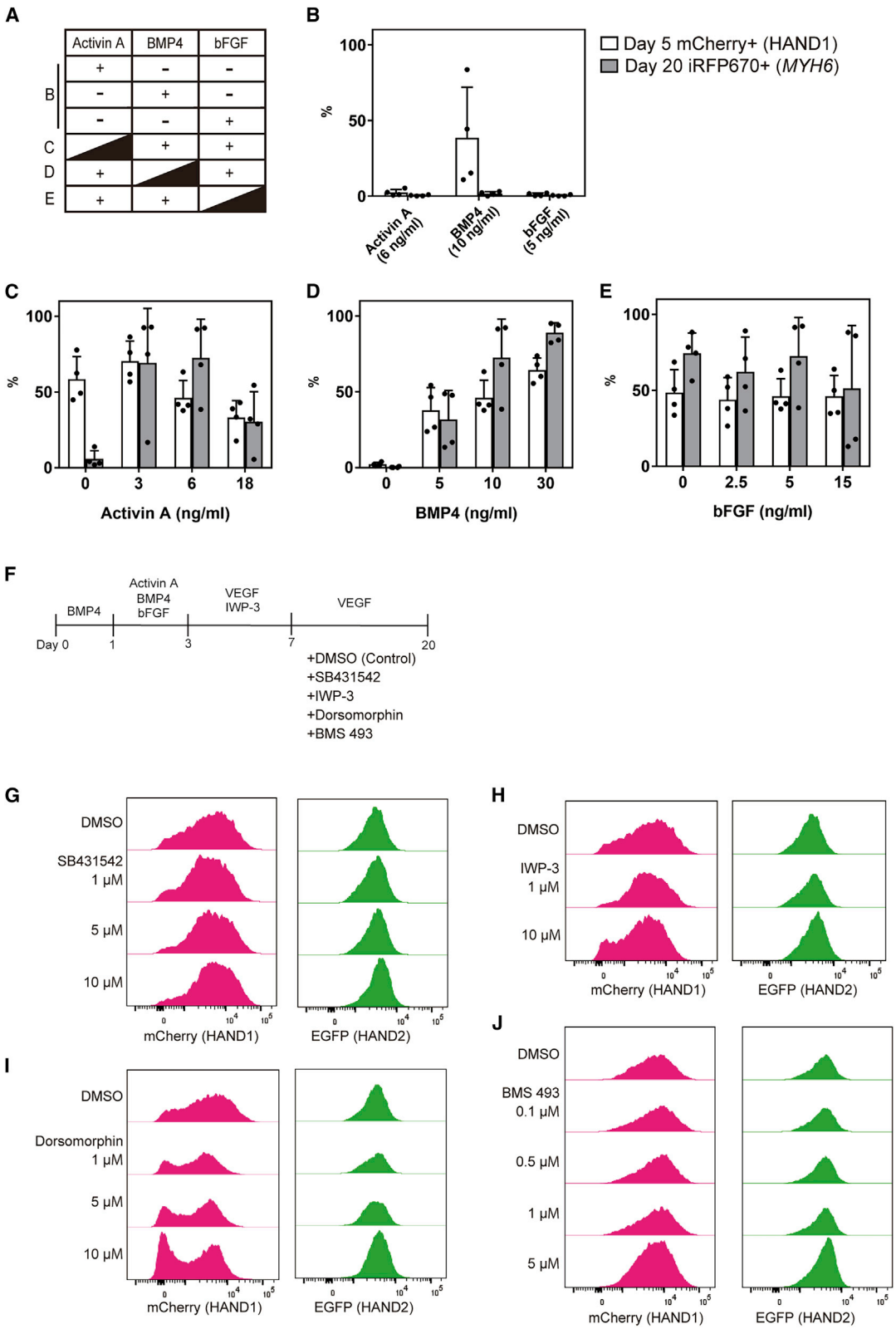

(legend on next page)

mCherry+ cells were maintained in the atrial protocol, but mCherry− cells were not, consistent with the ventricular protocol, suggesting that the expression of *HAND1* on day 5 marks CPCs in both conditions (Figure 4F).

To profile each subpopulation, we analyzed the RNA-seq data of day 20 iRFP670+ CMs in the four subpopulations from the ventricular induction protocol and the mCherry− EGFP+ population from the RA-modified (atrial) induction protocol (Figure 4G). The CMs generated from the atrial protocol showed a higher expression of atrial genes and lower expression of ventricular genes compared with all subpopulations from the ventricular protocol (Figure 4H), indicating mCherry− EGFP+ CMs prepared from the atrial protocol were atrial CMs. Because *HAND1* is widely expressed in the ventricle, although its expression is higher in the LV than RV (Figure 1H), we investigated if HAND1− (mCherry−) CMs of the ventricular protocol are RV-like CMs. No clear RV-specific expression patterns were observed in mCherry− CMs from the ventricular protocol (Figures 4I–4L). On the other hand, we found mCherry− EGFP+ atrial CMs had higher expressions of atrial genes, and mCherry+ EGFP+ CMs tended to have higher expressions of LV-specific genes.

Next we investigated the expression profiles of CMs induced in the monolayer culture. When iRFP670+ CMs were differentiated from day 5, the percentage of the mCherry− EGFP+ population was higher in EB-based CMs (Figures S5C–S5E), suggesting that monolayer CMs were a heterogeneous population of atrial and LV/RV CMs.

Profiling the four subpopulations of ventricular CMs

To characterize each ventricular subpopulation, we extracted differentially expressed genes and clustered them (Table S1). We found two major clusters, cluster 3 (1,276 genes) and cluster 4 (780 genes), which were highly expressed in mCherry+ CMs and mCherry− CMs, respectively (Figure 5A). A gene ontology (GO) analysis showed enriched GO terms for the cell cycle in cluster 3 (Figure 5B). Consistently, an enrichment analysis of Reactome pathways found cell cycle-related pathways were highly enriched in cluster 3 (Figures 5C and 5D and Table S2). Thus, we examined the 5-ethynil-2′-deoxyuridine (EdU) positive ratio of each subpopulation isolated from iRFP670+ CMs on day 20, finding that mCherry+ CMs showed significantly higher percentages of EdU+ cells than mCherry− CMs (Figures 5E and 5F). Previous studies indicated that CMs proliferate less in the mature heart during cardiogenesis *in vivo* and *in vitro* (Funakoshi et al., 2016; Takeuchi, 2014). Therefore, we investigated the maturation levels of the CM subpopulations by staining for α-actinin to observe the sarcomere structure and compared the expression levels of two immaturity-related genes, *MYH6* and *TNNI1*, and two maturation marker genes, *MYH7* and *TNNI3*, but found no clear difference between the four cell populations (Figures S5F and S5G) (Cui et al., 2019; Friedman et al., 2018). These results suggest that the expression of *HAND1* is correlated with the proliferation ability of CMs but not with the maturation level.

Regulatory network of CM proliferation

To understand the molecular mechanism determining highly and lowly proliferative CMs, we performed an upstream analysis of cluster three genes, which represent highly expressed genes in the mCherry+ population, using the geneXplain platform (Kel et al., 2006; Koschmann et al., 2015). As a result, a total of 103 TFs were predicted as upstream factors. Within these 103 TFs, *LEF1*, whose expression was significantly higher in mCherry+ EGFP+ CMs than mCherry− CMs, belongs to the same cluster as *HAND1*, indicating it has the most similar expression to *HAND1* during differentiation (day 0 to day 20) (Figures 6A and S6A). *LEF1* is a factor in the WNT signaling pathway and activates its target genes by cooperating with β-catenin (Clevers, 2006). Also in the enrichment analysis using the Reactome pathway, the WNT-related pathways "TCF dependent signaling in response to WNT" and "Signaling by WNT" were significantly enriched (Table S2) (Jassal et al., 2020). An analysis of RNA-seq data found that WNT signaling genes showed stage-specific expressions, including *LEF1* expression, which increased from day 5 (Figure S6B). Taken together, the upstream analysis of differentially expressed genes between HAND1+/− populations highlight the importance of WNT signaling in CM proliferation.

Figure 3. Effects of cytokines on *HAND1* and *HAND2* expression in ventricular and atrial differentiation

(A) Scheme of the cytokines in day 0–1 differentiation medium used for the experiments in (B)–(E).

(B) Percentages of mCherry+ cells on day 5 and iRFP670+ cells on day 20 with only Activin A, BMP4 or bFGF in day 0–1 medium (n = 4 independent experiments).

(C–E) Percentages of mCherry+ cells on day 5 and iRFP670+ CMs on day 20 cultured with various concentrations of Activin A (C), BMP4 (D), and bFGF (E) in day 0–1 medium (n = 4 independent experiments). All other cytokine concentrations followed the ventricular protocol. Data represent means ± SD.

(F) Scheme of the differentiation protocol for the experiments in (G)–(J).

(G–J) Representative histogram of mCherry and EGFP expressions on day 20 in iRFP670+ cells cultured with SB431542 (G), IWP-3 (H), dorsomorphin (I), and BMS 493 (J).

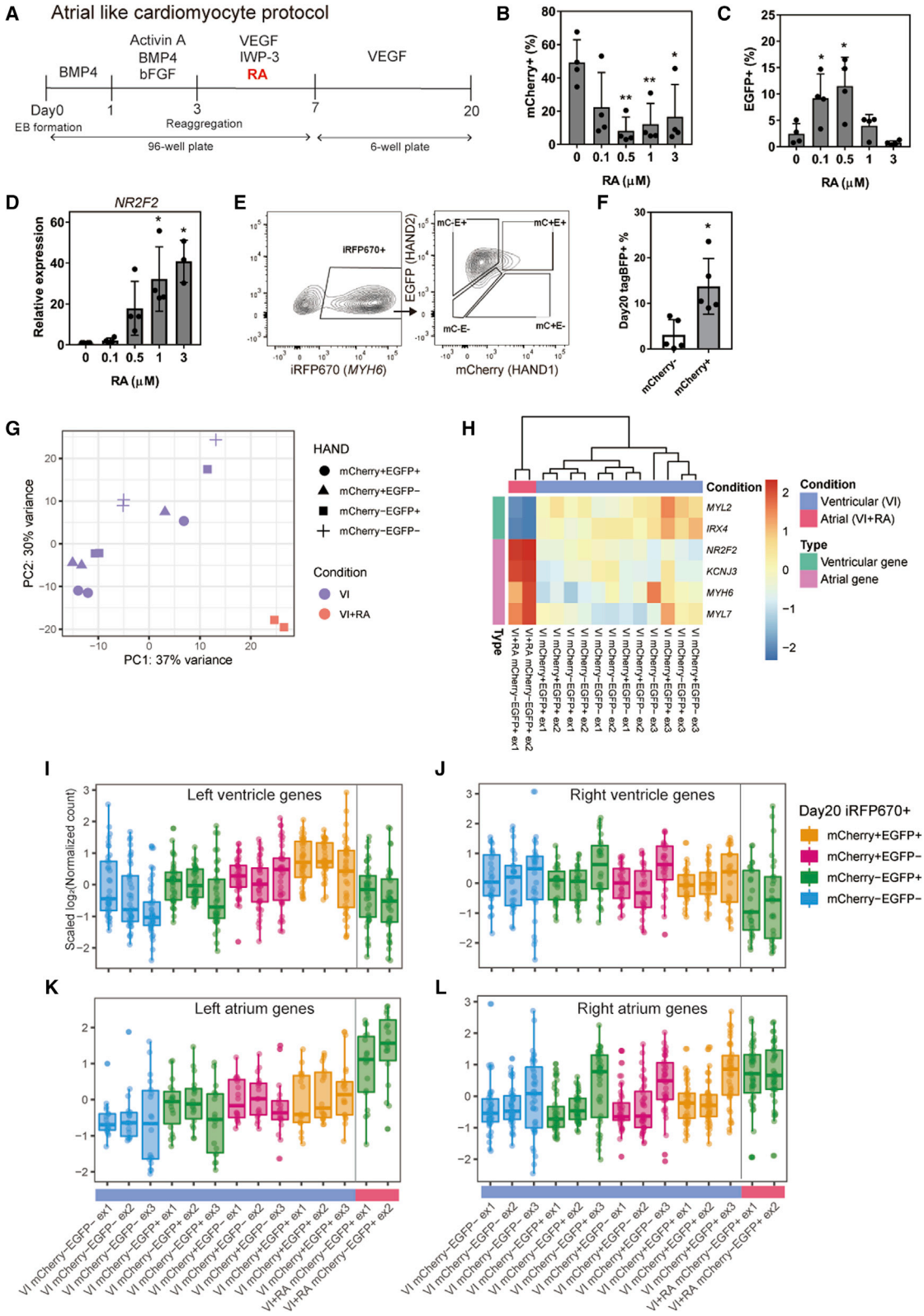

(legend on next page)

We therefore hypothesized that *HAND1*, *HAND2*, and *LEF1* control the cell cycle in CMs via WNT signaling. To test this hypothesis, a single CM reporter hiPSC line, 201B7 *MYH6*-EGFP, was differentiated and isolated on day 15 (Funakoshi et al., 2016). The CMs were then seeded and cultured in a dish until day 20 to investigate the direct effects of IWP-3 and CHIR99021 (CHIR), a GSK-3 inhibitor that induces lower β-catenin phosphorylation levels and enhances WNT signaling, from days 16 to 18. The administration of IWP-3 lowered the EdU+ ratio as well as the expression levels of *LEF1* (Figures 6B and 6C). Conversely, CHIR administration upregulated the EdU+ ratio and tended to increase the expression levels of *HAND1*, *HAND2*, and *LEF1* (Figures 6D and 6E).

To test the direct effects of *HAND1*, *HAND2*, and *LEF1* on the cell cycle in CMs, we used small interfering RNAs (-siRNAs) to knock down their expressions. *MYH6*-EGFP+ CMs were purified by FACS and transfected with siRNAs on day 15. The EdU+ ratio and expressions of *HAND1*, *HAND2*, and *LEF1* were measured on day 20 by real-time quantitative PCR (qPCR). The knockdown of *LEF1* caused a significant reduction in the EdU+ ratio, but the knockdown experiments of *HAND1* or *HAND2* did not (Figures 6F, 6G, S6C and S6D). We also performed an RNA-seq analysis of the three knockdowns to elucidate the effects of WNT signaling genes (Figure S6E). The knockdown of *HAND1* or *HAND2* did not change the expressions of WNT signaling genes. On the other hand, *CTNNB1*, *DKK3*, and *GSK3B* were downregulated by *LEF1* knockdown, as was *LEF1* itself (Figure S6E). Thus, only the knockdown of *LEF1* affected the expression levels of WNT signaling factors.

It was reported that the hypoplasia in *Hand1*- and *Hand2*-deficient mice is dose dependent (McFadden et al., 2005). Therefore, we next suppressed the expressions of *HAND1* and *HAND2* simultaneously but again found no change in the EdU+ ratio (Figure 6H). Finally, we found that the knockdown of *HAND2* caused a significant reduction in the EdU+ ratio if WNT signaling was activated by CHIR, suggesting a proliferation role of *HAND2* (Figure 6I). However, the knockdown of *HAND1* did not show this effect. This difference may be attributable to the higher frequency of HAND2+ CMs compared with HAND1+ CMs.

Interestingly, the *HAND1* and *HAND2* knockdown experiments significantly enhanced the expression of *LEF1*, while conversely the *LEF1* knockdown significantly increased the expressions of *HAND1* and *HAND2* (Figure 6G). These observations suggested that *HAND1* and *HAND2* regulate *LEF1* expression and that *LEF1* regulates *HAND1* and *HAND2* expression. We checked these direct regulations using published chromatin immunoprecipitation sequencing (ChIP-seq) data (Table S3) (Boeva et al., 2017; Consortium, 2012; Durbin et al., 2018; Hemming et al., 2018; Tsankov et al., 2015). We found HAND1 and HAND2 bind upstream of the *LEF1* locus without active histone mark (H3K27Ac), especially in human cell lines, including GIST-T1, BE2C, CLB-Ga, K562, and HEK293, and human embryonic stem cell (ESC)-derived mesodermal cells on day 5, suggesting HAND1 and HAND2 directly downregulate *LEF1* expression by binding to the upstream region (Figure S6F). The ChIP-seq data also indicated that HAND1, HAND2, and LEF1 directly bind to the loci of *CCND1* and *CCND2*, two cell cycle regulators. The overexpression of *CCND1* induces human CMs to proliferate (Mohamed et al., 2018). Furthermore, the data showed that LEF1 binds to the upstream loci of *HAND1* and *HAND2*. Overall, these data suggest that a gene regulatory network for the proliferation of CMs involves the binding of HAND1, HAND2, and LEF1 to each other's loci.

CD105 is a marker of highly proliferative CMs

To further investigate the relationship between CM proliferation and cardiac TFs in CMs, we focused on marker proteins for proliferative CMs. We picked up cell surface genes among the differentially expressed genes from our RNA-seq

Figure 4. Retinoic acid in the atrial protocol upregulated *HAND2* and downregulated *HAND1*

(A) Scheme of the RA-modified atrial CM differentiation protocol.

(B and C) Percentages of mCherry+ cells (B) and EGFP+ cells (C) on day 7 at different RA concentrations (n = 4 independent experiments). *p < 0.05, **p < 0.01 by one-way ANOVA with Dunnett's test comparing with 0 μM.

(D) Gene expression level of *NR2F2*, an atrial marker gene, on day 7 at different RA concentrations. (n = 3–4 independent experiments). *p < 0.05, **p < 0.01 by one-way ANOVA with Dunnett's test comparing with 0 μM.

(E) Representative FACS plots of iRFP670, mCherry (mC), and EGFP (E) expressions on day 20 (n = 5 independent experiments).

(F) Percentages of tagBFP+ cells on day 20. EBs were mixed with tagBFP+ mCherry+ cells and tagBFP− cells or with tagBFP+ mCherry− cells and tagBFP− cells on day 5 (n = 3 independent experiments). *p < 0.05 by unpaired t test. Data represent means ± SD.

(G) Principal component analysis plot of ventricular CMs (VEGF + IWP-3 on day 3; VI) and atrial CMs (VEGF + IWP-3 + RA on day 3; VI + RA) (n = 3 independent experiments).

(H) Heatmap of scaled expression levels of *MYL7*, *MYH6*, *KCNJ3*, and *NR2F2* (atrial marker genes) and *MYL2* and *IRX4* (ventricular marker genes) from the RNA-seq data of day 20 CMs.

(I–L) Box plots of the scaled $\log_2$ normalized counts of chamber-specific genes in each subpopulation. The upper and lower quartiles are indicated by the boxes, and the median by the lines within each box.

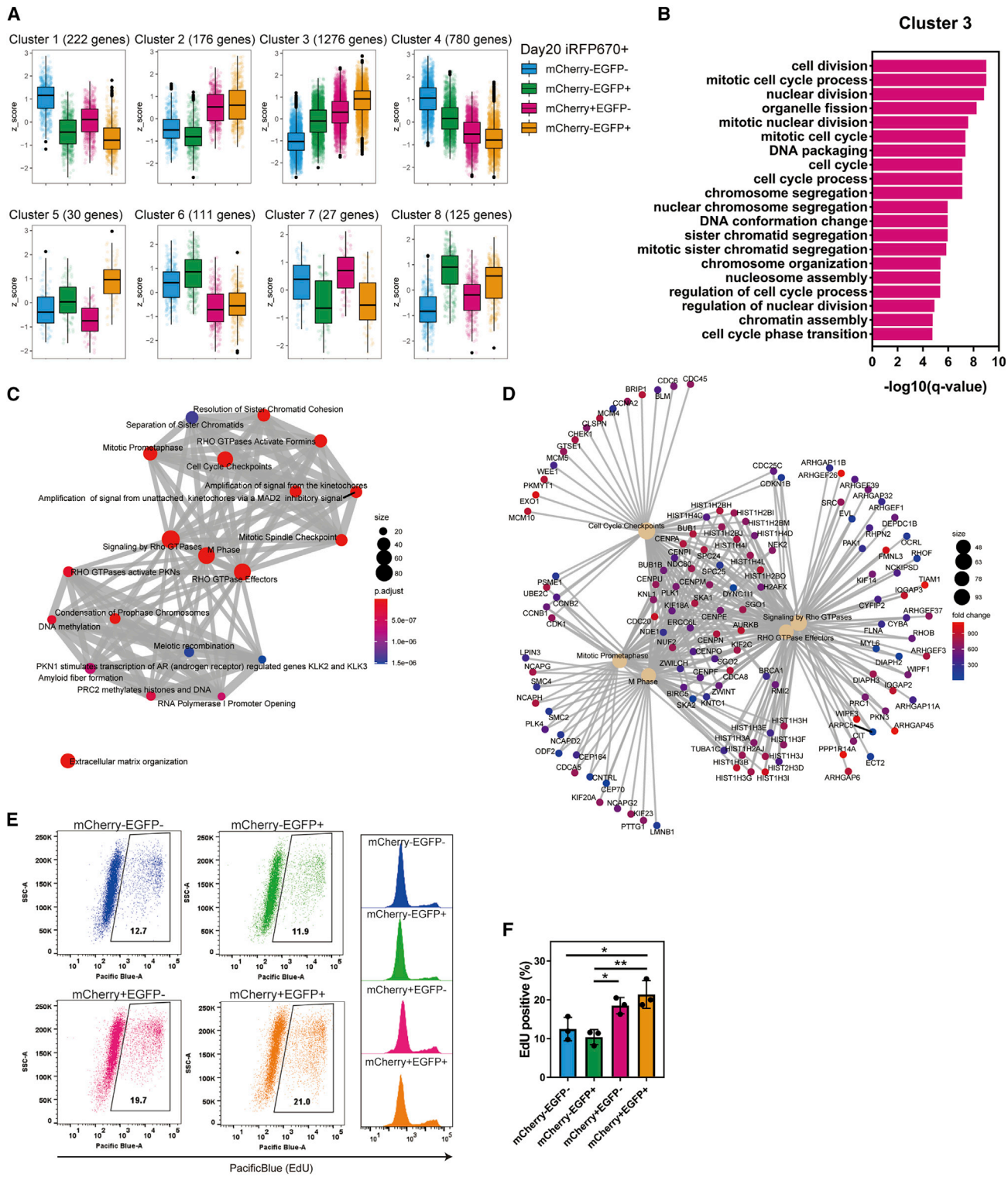

Figure 5. Characterization of subpopulations isolated from iRFP670+ CMs on day 20

(A) Genes that showed a significant expression difference between the four subpopulations based on the likelihood ratio test (adjustment p value <0.05) were clustered into eight clusters. Box plots of the scaled values (*Z* score) show the upper and lower quartiles by boxes and the median as a line within each box.

(legend continued on next page)

data in the CM subpopulations. CD105 (also known as endoglin, encoded by *ENG*) showed a higher expression in mCherry+ CMs (Figure 7A). We sorted CD105-high (top 30%) and CD105-low (bottom 30%) populations from EGFP+ CMs on day 20 (Figure 7B). The EdU+ ratio and *HAND1* expression level of CD105-high CMs were higher than those of CD105-low CMs (Figures 7C and 7D). We also tested the utility of CD105 to sort lineage (CD31, CD49a, CD140b, CD90)-negative and signal regulatory protein alpha (SIRPA)-positive CMs derived from 692D2 (on-feeder hiPSC line) and 1390D4 (feeder-free hiPSC line). We found a high EdU ratio in the CD105+ population, which also showed a high expression level of *HAND1* (Figures S7A–S7D). CD105 is a TGFβ receptor (Arthur et al., 2000). Therefore, we investigated whether TGFβ signaling is associated with cell cycle activity by adding SB431542 on days 16–18 to the isolated CMs. The inhibitor caused no change in the EdU+ ratio (Figures S7E and S7F), suggesting that TGFβ signaling is not involved in cell cycle regulation.

Taken together, our *in vitro* differentiation model of the expression dynamics of *HAND1* and *HAND2* (Figure S7G) highlights a cell cycle regulation system involving *LEF1*, *HAND1*, and *HAND2* and revealed CD105 as a marker of proliferative CMs.

DISCUSSION

HiPSC reporter systems are useful tools for assessing the developmental mechanisms of cardiogenesis. These systems can clarify the role of cardiac TFs by tracing and profiling cell subpopulations. Previously, studies using *Tbx1/Hcn4* and *TBX5/NKX2-5* double-reporter iPSC lines investigated the dynamics of these genes and subpopulations (Andersen et al., 2018; Zhang et al., 2019). However, the expression dynamics of *HAND1* and *HAND2* in human cardiogenesis still remain to be clarified. In this study, we established a *HAND1/HAND2* double-reporter hiPSC line and investigated the expression dynamics of the two TFs during cardiac differentiation for the first time.

According to a previous study investigating gene expressions, heart cell types develop differently between human and mouse *in vivo* (Cui et al., 2019). In mice, the expressions of both *Hand1* and *Hand2* begin from LPM, and there is little spatial overlap between the two in the heart tube (Cserjesi et al., 1995; de Soysa et al., 2019; Srivastava et al., 1997). On the other hand, we observed that the expression of HAND1-mCheery in hiPSCs started from day 3 of the differentiation, which is the mesodermal stage, and the expression of HAND2-EGFP started between days 5 and 7, demonstrating the difference between human *in vitro* and mouse *in vivo* differentiation.

According to the gene expression profiles of ventricular CMs, our reporter did not show evidence of RV CM differentiation. One reason could be that the HAND1− CM subpopulation on day 20 is heterogeneous. Another possible reason is that our ventricular protocol did not produce RV CMs. Protze et al. (2019) hypothesized that RV CMs are generated from a low Activin A concentration, but experimental confirmation is still awaited. Thus, more study on the different cellular properties of LV and RV CMs is needed in order to produce RV CMs *in vitro*.

Previous reports have shown that CHIR via canonical WNT signaling can enhance the proliferation of CMs derived from hiPSCs (Buikema et al., 2020; Mills et al., 2019). In the present study, we found *LEF1* expression is a key transcriptional regulator of the cell cycle in CMs. In mice, *Lef1* is a canonical WNT signaling factor detected in embryonic heart transiently at E13.5–E17.5 and directly binds to the promoter region of *CCND2* and *CCND1* (Shtutman et al., 1999; Ye et al., 2019), which are required for the progression of G1 in the cell cycle. These previous reports as well as our findings support the direct regulation of *LEF1* and cell cycle progression in CMs under WNT signaling.

Some previous reports have shown that *Hand1* overexpression and conditional knockout cause overgrowth of the heart tube and smaller LV size, respectively, in mice, indicating *Hand1* promotes proliferation (McFadden et al., 2005; Risebro et al., 2006). Recently, an LV-specific *Hand1* enhancer was identified, and LV-specific *Hand1*-deficient mice from that study had a similar phenotype to the aforementioned conditional knockout mice (McFadden et al., 2005; Vincentz et al., 2017). However, LV-specific *Hand1* and *Hand2* dual-deficient mice showed an overgrowth of the myocardium, suggesting *Hand1* and *Hand2* suppress the proliferation of CMs (Vincentz et al., 2017). Thus, mouse studies indicate that *Hand1* and *Hand2* can both promote and suppress proliferation in a context-dependent manner. In the present study, we observed that the knockdown of *HAND1* did not change the EdU+ ratio, but *HAND2* or *LEF1* knockdown reduced the

(B) Top 20 enriched GO terms in biological process for the genes in cluster 3.
(C) Enrichment map of the Reactome pathway from the gene set enrichment analysis using the genes in cluster 3.
(D) Network plot of the most significantly enriched terms with the genes in cluster 3.
(E) Representative FACS plot of EdU assays.
(F) Percentages of EdU+ cells in each subpopulation isolated on day 20 (n = 3 independent experiments). *$p < 0.05$, **$p < 0.01$ by one-way ANOVA with Tukey's multiple comparisons test. Data represent means ± SD.

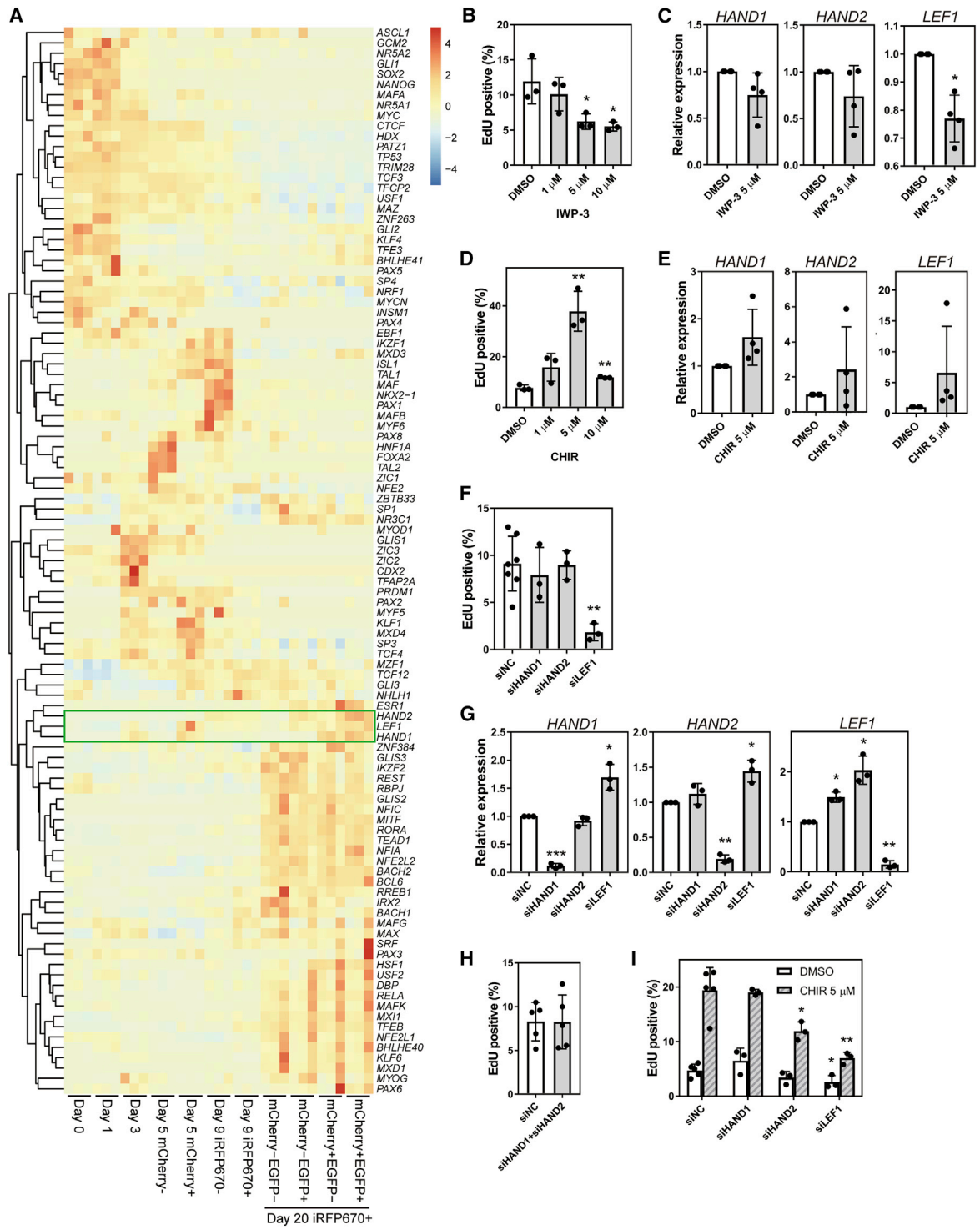

Figure 6. WNT signaling and proliferation in CMs

(A) Heatmap and clustering of scaled expression levels of 103 TFs predicted as upstream factors from the RNA-seq data of days 0, 3, 5 (isolated mCherry− and mCherry+ populations), day 9 (isolated iRFP670− and iRFP670+ populations), and day 20 subpopulations in iRFP670+ CMs (n = 3 independent experiments). Green box highlights *HAND1*, *LEF1*, and *HAND2*.

(B) Percentage of EdU+ cells on day 20 among EGFP+ CMs isolated on day 15 following WNT inhibitor (IWP-3) administration on days 16–18 (n = 3 independent experiments). *p < 0.05 by one-way ANOVA with Dunnett's test comparing with DMSO.

(legend continued on next page)

proliferation. Also, we observed that the expression of *LEF1* was upregulated by the knockdown of *HAND1* and *HAND2*, indicating the expression of *HAND1* and *HAND2* suppresses CM proliferation. These findings suggest a gene regulatory network of the cell cycle in CMs for precise cell proliferation depends on *HAND1*, *HAND2*, and *LEF1*.

Finally, we found CD105 as a marker of highly proliferative CMs. *CD105* is highly expressed in endothelial and mesenchymal cells and also a TGFβ signaling receptor. Its deficiency in mouse is embryonic lethal as a result of cardiovascular abnormalities (Arthur et al., 2000), but little is known about *CD105* function in human CMs. In the present study, TGFβ signaling inhibition did not change the proliferation capacity of CMs, suggesting that *CD105* has little functional contribution to the proliferation as a TGFβ signaling receptor even though it can act as marker of proliferative CMs.

To conclude, our results indicate that *HAND1* has different roles in the early and late stages of *in vitro* differentiation. The first expression of *HAND1*, on day 3–5 (early stage), is induced by BMP4. Our tracing system showed that *HAND1* marks CPCs in both our ventricular and atrial protocols, suggesting its role in the cell fate decision to CMs. In the later stage, our data indicated that *HAND1* and *HAND2* regulate *LEF1* to affect the proliferation capacity of CMs via WNT signaling. Of note, atrial CMs showed a strong expression of *HAND2* and little expression of *HAND1*, suggesting that regulatory mechanisms for the proliferation of atrial CMs are different from those of ventricular CMs. We also found evidence that CD105 is a marker of proliferative CMs. However, further molecular analysis is needed to reveal how *HAND1* and *HAND2* repress *LEF1* and how the three factors orchestrate the development of the four-chambered heart morphology during cardiac organogenesis.

EXPERIMENTAL PROCEDURES

Establishment of triple-reporter lines

To establish the *HAND1*^{mCherry} and *HAND2*^{EGFP} double-reporter line, the CRISPR-Cas9 system was used to knock in a FLAG-2A-mCherry cassette (floxed PGK-puromycin resistance) and an HA-2A-EGFP cassette (floxed-PGK-neomycin resistance) at the *HAND1* and *HAND2* loci, respectively. To establish the triple-reporter line with constitutive tagBFP expression in addition to the double-reporter line, a CAG-tagBFP cassette for AAVS1 was knocked in using TALEN. All vectors of these knockin experiments were transfected into hiPSCs by electroporation with an NEPA 21 (NEPAGENE) following a previously described method with modifications (Li et al., 2015). *MYH6*-EGFP reporter hiPSCs were established as previously reported (Funakoshi et al., 2016). In this study, we modified the *MYH6*-EGFP *piggyBac* vector to change the EGFP coding sequence to an iRFP670 coding sequence. All DNA oligos/primers and vectors are listed in Table S4, and detailed protocols are described in the supplemental information.

hiPSC culture and cardiomyocyte induction

The cell culture and induction protocol for ventricular CMs were done as reported previously, with some modification (Funakoshi et al., 2016; Yang et al., 2008). Specifically, we alternatively used 96-well and 6-well plates coated with poly(2-hydroxyethyl methacrylate) (HEMA, Sigma-Aldrich). The atrial differentiation protocol was the same except 0.5 μM all-*trans* RA (Wako) was added to the day 3 medium. The use of hiPSCs were approved by the Ethics Committee of Kyoto University.

Flow cytometry and immunostaining

All analysis and sorting were performed with FACS AriaII (Becton Dickinson) and analyzed by FlowJo (Becton Dickinson). All antibodies are listed in Table S5, and detailed protocols are described in the supplemental information.

RNA extraction and real-time qPCR

RNA was purified using QIAZOL reagent and the miRNeasy Micro Kit (QIAGEN), and cDNA was synthesized using ReverTra Ace (TOYOBO) with poly T primer or ReverTra Ace qPCR RT Master Mix with gDNA Remover (TOYOBO). Transcripts were amplified using the TaqMan probes (Applied Biosystems) listed in Table S6 and TaqMan Universal Master Mix II with Uracil-N-glycosylase (UNG) (Applied Biosystems). Real-time qPCR analysis was performed using StepOne (Applied Biosystems). Gene expression levels were calculated using the $2^{-\Delta\Delta CT}$ method with GAPDH or ACTB as the reference gene.

(C) Real-time qPCR results for *HAND1*, *HAND2*, and *LEF1* expression under IWP-3 treatment (n = 4 independent experiments). *p < 0.05, by Welch's t test.
(D) Percentage of EdU+ cells on day 20 among EGFP+ CMs isolated on day 15 following GSK3 inhibitor CHIR99021 (CHIR) administration on days 16–18 (n = 3 independent experiments). ***p < 0.001 by one-way ANOVA with Dunnett's test comparing with DMSO.
(E) Real-time qPCR results of *HAND1*, *HAND2*, and *LEF1* expression under CHIR treatment (n = 4 independent experiments).
(F) Percentage of EdU+ cells after treatment with siRNAs for negative control (siNC), *HAND1* (siHAND1), *HAND2* (siHAND2), and *LEF1* (siLEF1) (n = 3–7 independent experiments). **p < 0.01 by one-way ANOVA with Dunnett's test comparing with siNC.
(G) Real-time qPCR results for *HAND1*, *HAND2*, and *LEF1* expression after siRNA treatment on day 20. EGFP+ CMs isolated on day 15 (n = 3 independent experiments). *p < 0.05, **p < 0.01, ***p < 0.001 by Welch's t test.
(H) Percentage of EdU+ cells with simultaneous knockdown of *HAND1* and *HAND2* (n = 5 independent experiments).
(I) Percentage of EdU+ cells after CHIR and siRNA combination treatment (n = 3–5 independent experiments). *p < 0.05, ***p < 0.001 by one-way ANOVA with Dunnett's test comparing with siNC. Data represent means ± SD.

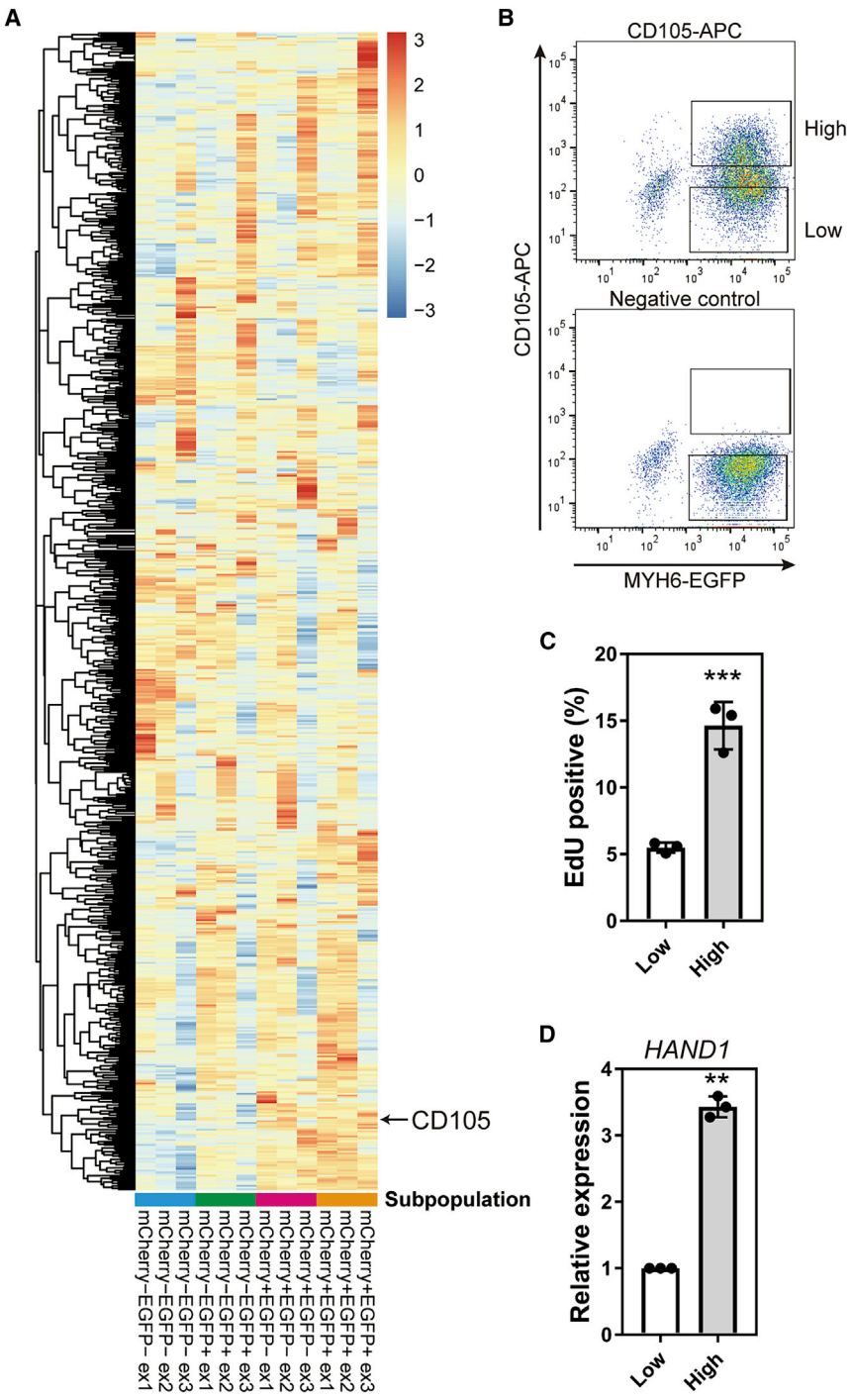

Figure 7. Identification of CD105 as a surface marker of proliferative CMs

(A) Heatmap of the expression level of cell surface (GO: 0009986) genes in each subpopulation of CMs on day 20 by RNA-seq data.

(B) Representative FACS plots of *MYH6*-EGFP reporter hiPSCs (201B7) using CD105-APC antibody on day 20. CD105-high and CD105-low populations were isolated from the upper 30% and lower 30% of EGFP+ CMs, respectively.

(C) Percentages of EdU+ cells on day 23 in EGFP+ and CD105-APC-high or -low CMs isolated on day 20 (n = 3 independent experiments). ***p < 0.001 by unpaired t test.

(D) Expression level of *HAND1* in CD105-high and -low CMs isolated on day 20 (n = 3 independent experiments). **p < 0.01 by Welch's t test. Data represent means ± SD.

Knockdown experiments

For knockdown, the reverse transfection method was used with Lipofectamine RNAiMAX Reagent (Invitrogen) following the manufacturer's instructions. On day 15, 5 nmol of each siRNA (Silencer Select, Ambion) was transfected into isolated *MYH6*-EGFP+ CMs as single-cell suspensions (Table S7). The suspensions were seeded at 3–4 × 10^5 cells/well on a fibronectin-coated 12-well plate. On day 16, the medium was refreshed. On day 20, the cells were collected with QIAZOL and M-PER (Thermo).

RNA-seq and data analysis

Details of the experiment procedure and analysis are described in the supplemental information.

Statistics

GraphPad Prism (Version 7.05) was used to statistically analyze EdU data and gene expression data. All bar charts with error bars represent means ± standard deviation (SD).

Data and code availability

The accession number for the RNA-seq reported in this paper is GEO: GSE156394.

SUPPLEMENTAL INFORMATION

Supplemental information can be found online at https://doi.org/10.1016/j.stemcr.2021.06.014.

AUTHOR CONTRIBUTIONS

C.O. and Y.Y. conceived this project and wrote the manuscript. C.O. performed the computational and experimental analyses. A.H. supported the CRISPR experiments. S.Y. supervised the project. A.I., M. Nishikawa, and M. Narita helped with the experimental analyses. All authors contributed to the final article.

CONFLICTS OF INTERESTS

S.Y. is a scientific advisor without salary of iPS Academia Japan, Inc. and Altos Labs, Inc. Y.Y. receives a research grant from Takeda Pharmaceutical Company Ltd. Kyoto University has filed a patent application relevant to this work. C.O and Y.Y are the investigators of record listed on the patent application.

ACKNOWLEDGMENTS

We thank Dr. Peter Karagiannis for critical reading of the manuscript, Dr. Knut Woltjen for supporting experiments using the *piggyBac* transposon and TALEN, Dr. Takuya Yamamoto for providing some scripts and advice for the RNA-seq analysis, Dr. Kanae Mitsunaga for providing advice on the FACS analysis, Mr. Shunsuke Kihara for performing the confocal imaging, Dr. Hirohide Saito for providing the template oligos of tagBFP and iRFP670, and Dr. Keisuke Okita for providing the Cre expression vector. We are also grateful to Ms. Sayaka Takeshima, Ms. Yoko Uematsu, and Ms. Kaoru Shimizu for their administrative support. This work was supported by Japan Society for the Promotion of Science (JSPS) KAKENHI 16J02610 to C.O. and 17H04176 to Y.Y. This work was also supported by The Leducq Foundation (18CVD05), the Research Center Network for Realization of Regenerative Medicine, Japan Agency for Medical Research and Development (AMED) (JP19bm0104001, JP19bm0204003, JP19bm0804008, and JP20bm0804022), the Research on Regulatory Science of Pharmaceuticals and Medical Devices, AMED (JP19mk0104117), the Research Project for Practical Applications of Regenerative Medicine, AMED (JP19bk0104095), the iPS Cell Research Fund, and the Secom Science and Technology Foundation.

Received: November 6, 2020
Revised: June 22, 2021
Accepted: June 23, 2021
Published: July 22, 2021

REFERENCES

Andersen, P., Tampakakis, E., Jimenez, D.V., Kannan, S., Miyamoto, M., Shin, H.K., Saberi, A., Murphy, S., Sulistio, E., Chelko, S.P., et al. (2018). Precardiac organoids form two heart fields via Bmp/Wnt signaling. Nat. Commun. *9*, 3140.

Arthur, H.M., Ure, J., Smith, A.J., Renforth, G., Wilson, D.I., Torsney, E., Charlton, R., Parums, D.V., Jowett, T., Marchuk, D.A., et al. (2000). Endoglin, an ancillary TGFbeta receptor, is required for extraembryonic angiogenesis and plays a key role in heart development. Dev. Biol. *217*, 42–53.

Barnes, R.M., Firulli, B.A., Conway, S.J., Vincentz, J.W., and Firulli, A.B. (2010). Analysis of the Hand1 cell lineage reveals novel contributions to cardiovascular, neural crest, extra-embryonic, and lateral mesoderm derivatives. Dev. Dyn. *239*, 3086–3097.

Boeva, V., Louis-Brennetot, C., Peltier, A., Durand, S., Pierre-Eugene, C., Raynal, V., Etchevers, H.C., Thomas, S., Lermine, A., Daudigeos-Dubus, E., et al. (2017). Heterogeneity of neuroblastoma cell identity defined by transcriptional circuitries. Nat. Genet. *49*, 1408–1413.

Bruneau, B.G., Logan, M., Davis, N., Levi, T., Tabin, C.J., Seidman, J.G., and Seidman, C.E. (1999). Chamber-specific cardiac expression of Tbx5 and heart defects in Holt-Oram syndrome. Dev. Biol. *211*, 100–108.

Buikema, J.W., Lee, S., Goodyer, W.R., Maas, R.G., Chirikian, O., Li, G., Miao, Y., Paige, S.L., Lee, D., Wu, H., et al. (2020). Wnt activation and reduced cell-cell contact synergistically induce massive expansion of functional human iPSC-derived cardiomyocytes. Cell Stem Cell *27*, 50–63.e55.

Burridge, P.W., Keller, G., Gold, J.D., and Wu, J.C. (2012). Production of de novo cardiomyocytes: human pluripotent stem cell differentiation and direct reprogramming. Cell Stem Cell *10*, 16–28.

Cai, C.L., Liang, X., Shi, Y., Chu, P.H., Pfaff, S.L., Chen, J., and Evans, S. (2003). Isl1 identifies a cardiac progenitor population that proliferates prior to differentiation and contributes a majority of cells to the heart. Dev. Cell *5*, 877–889.

Clevers, H. (2006). Wnt/beta-catenin signaling in development and disease. Cell *127*, 469–480.

Consortium, E.P. (2012). An integrated encyclopedia of DNA elements in the human genome. Nature *489*, 57–74.

Cserjesi, P., Brown, D., Lyons, G.E., and Olson, E.N. (1995). Expression of the novel basic helix-loop-helix gene eHAND in neural crest derivatives and extraembryonic membranes during mouse development. Dev. Biol. *170*, 664–678.

Cui, Y.L., Zheng, Y.X., Liu, X.X., Yan, L.Y., Fan, X.Y., Yong, J., Hu, Y.Q., Dong, J., Li, Q.Q., Wu, X.L., et al. (2019). Single-cell transcriptome analysis maps the developmental track of the human heart. Cell Rep. *26*, 1934.

de Soysa, T.Y., Ranade, S.S., Okawa, S., Ravichandran, S., Huang, Y., Salunga, H.T., Schricker, A., del Sol, A., Gifford, C.A., and Srivastava, D. (2019). Single-cell analysis of cardiogenesis reveals basis for organ-level developmental defects. Nature *572*, 120.

Devalla, H.D., Schwach, V., Ford, J.W., Milnes, J.T., El-Haou, S., Jackson, C., Gkatzis, K., Elliott, D.A., Chuva de Sousa Lopes, S.M., Mummery, C.L., et al. (2015). Atrial-like cardiomyocytes

from human pluripotent stem cells are a robust preclinical model for assessing atrial-selective pharmacology. EMBO Mol. Med. *7*, 394–410.

Durbin, A.D., Zimmerman, M.W., Dharia, N.V., Abraham, B.J., Iniguez, A.B., Weichert-Leahey, N., He, S., Krill-Burger, J.M., Root, D.E., Vazquez, F., et al. (2018). Selective gene dependencies in MYCN-amplified neuroblastoma include the core transcriptional regulatory circuitry. Nat. Genet. *50*, 1240–1246.

Firulli, A.B., McFadden, D.G., Lin, Q., Srivastava, D., and Olson, E.N. (1998). Heart and extra-embryonic mesodermal defects in mouse embryos lacking the bHLH transcription factor Hand1. Nat. Genet. *18*, 266–270.

Friedman, C.E., Nguyen, Q., Lukowski, S.W., Helfer, A., Chiu, H.S., Miklas, J., Levy, S., Suo, S., Han, J.J., Osteil, P., et al. (2018). Single-cell transcriptomic analysis of cardiac differentiation from human PSCs reveals HOPX-dependent cardiomyocyte maturation. Cell Stem Cell *23*, 586–598.e8.

Funakoshi, S., Miki, K., Takaki, T., Okubo, C., Hatani, T., Chonabayashi, K., Nishikawa, M., Takei, I., Oishi, A., Narita, M., et al. (2016). Enhanced engraftment, proliferation, and therapeutic potential in heart using optimized human iPSC-derived cardiomyocytes. Sci. Rep-uk *6*. https://doi.org/10.1038/srep19111.

Garry, D.J., and Olson, E.N. (2006). A common progenitor at the heart of development. Cell *127*, 1101–1104.

George, R.M., and Firulli, A.B. (2019). Hand factors in cardiac development. Anat. Rec. (Hoboken) *302*, 101–107.

Hemming, M.L., Lawlor, M.A., Zeid, R., Lesluyes, T., Fletcher, J.A., Raut, C.P., Sicinska, E.T., Chibon, F., Armstrong, S.A., Demetri, G.D., et al. (2018). Gastrointestinal stromal tumor enhancers support a transcription factor network predictive of clinical outcome. Proc. Natl. Acad. Sci. U S A *115*, E5746–E5755.

Hochgreb, T., Linhares, V.L., Menezes, D.C., Sampaio, A.C., Yan, C.Y., Cardoso, W.V., Rosenthal, N., and Xavier-Neto, J. (2003). A caudorostral wave of RALDH2 conveys anteroposterior information to the cardiac field. Development *130*, 5363–5374.

Jassal, B., Matthews, L., Viteri, G., Gong, C., Lorente, P., Fabregat, A., Sidiropoulos, K., Cook, J., Gillespie, M., Haw, R., et al. (2020). The reactome pathway knowledgebase. Nucleic Acids Res. *48*, D498–D503.

Kattman, S.J., Witty, A.D., Gagliardi, M., Dubois, N.C., Niapour, M., Hotta, A., Ellis, J., and Keller, G. (2011). Stage-specific optimization of activin/nodal and BMP signaling promotes cardiac differentiation of mouse and human pluripotent stem cell lines. Cell Stem Cell *8*, 228–240.

Kel, A., Voss, N., Jauregui, R., Kel-Margoulis, O., and Wingender, E. (2006). Beyond microarrays: finding key transcription factors controlling signal transduction pathways. Bmc Bioinformatics *7*.

Koschmann, J., Bhar, A., Stegmaier, P., Kel, A.E., and Wingender, E. (2015). Upstream analysis": an integrated promoter-pathway analysis approach to causal interpretation of microarray data. Microarrays (Basel) *4*, 270–286.

Lee, J.H., Protze, S.I., Laksman, Z., Backx, P.H., and Keller, G.M. (2017). Human pluripotent stem cell-derived atrial and ventricular cardiomyocytes develop from distinct mesoderm populations. Cell Stem Cell *21*, 179–194.e4.

Li, H.L., Fujimoto, N., Sasakawa, N., Shirai, S., Ohkame, T., Sakuma, T., Tanaka, M., Amano, N., Watanabe, A., Sakurai, H., et al. (2015). Precise correction of the dystrophin gene in Duchenne muscular dystrophy patient induced pluripotent stem cells by TALEN and CRISPR-Cas9. Stem Cell Reports *4*, 143–154.

Mali, P., Yang, L., Esvelt, K.M., Aach, J., Guell, M., DiCarlo, J.E., Norville, J.E., and Church, G.M. (2013). RNA-guided human genome engineering via Cas9. Science *339*, 823–826.

McFadden, D.G., Barbosa, A.C., Richardson, J.A., Schneider, M.D., Srivastava, D., and Olson, E.N. (2005). The Hand1 and Hand2 transcription factors regulate expansion of the embryonic cardiac ventricles in a gene dosage-dependent manner. Development *132*, 189–201.

Meilhac, S.M., and Buckingham, M.E. (2018). The deployment of cell lineages that form the mammalian heart. Nat. Rev. Cardiol. *15*, 705–724.

Mills, R.J., Parker, B.L., Quaife-Ryan, G.A., Voges, H.K., Needham, E.J., Bornot, A., Ding, M., Andersson, H., Polla, M., Elliott, D.A., et al. (2019). Drug screening in human PSC-cardiac organoids identifies pro-proliferative compounds acting via the mevalonate pathway. Cell Stem Cell *24*, 895–907.e6.

Mohamed, T.M.A., Ang, Y.S., Radzinsky, E., Zhou, P., Huang, Y., Elfenbein, A., Foley, A., Magnitsky, S., and Srivastava, D. (2018). Regulation of cell cycle to stimulate adult cardiomyocyte proliferation and cardiac regeneration. Cell *173*, 104–116.e2.

Protze, S.I., Lee, J.H., and Keller, G.M. (2019). Human pluripotent stem cell-derived cardiovascular cells: from developmental biology to therapeutic applications. Cell Stem Cell *25*, 311–327.

Randolph, L.N., and Lian, X.L. (2019). Beyond purple hearts: a colorful approach to isolate distinct heart cells from human iPSCs. Cell Stem Cell *24*, 675–677.

Reamon-Buettner, S.M., Ciribilli, Y., Inga, A., and Borlak, J. (2008). A loss-of-function mutation in the binding domain of HAND1 predicts hypoplasia of the human hearts. Hum. Mol. Genet. *17*, 1397–1405.

Reamon-Buettner, S.M., Ciribilli, Y., Traverso, I., Kuhls, B., Inga, A., and Borlak, J. (2009). A functional genetic study identifies HAND1 mutations in septation defects of the human heart. Hum. Mol. Genet. *18*, 3567–3578.

Riley, P., Anson-Cartwright, L., and Cross, J.C. (1998). The Hand1 bHLH transcription factor is essential for placentation and cardiac morphogenesis. Nat. Genet. *18*, 271–275.

Risebro, C.A., Smart, N., Dupays, L., Breckenridge, R., Mohun, T.J., and Riley, P.R. (2006). Hand1 regulates cardiomyocyte proliferation versus differentiation in the developing heart. Development *133*, 4595–4606.

Rochais, F., Mesbah, K., and Kelly, R.G. (2009). Signaling pathways controlling second heart field development. Circ. Res. *104*, 933–942.

Shtutman, M., Zhurinsky, J., Simcha, I., Albanese, C., D'Amico, M., Pestell, R., and Ben-Ze'ev, A. (1999). The cyclin D1 gene is a target of the beta-catenin/LEF-1 pathway. Proc. Natl. Acad. Sci. U S A *96*, 5522–5527.

Singh, M.K., Christoffels, V.M., Dias, J.M., Trowe, M.O., Petry, M., Schuster-Gossler, K., Burger, A., Ericson, J., and Kispert, A. (2005).

Tbx20 is essential for cardiac chamber differentiation and repression of Tbx2. Development *132*, 2697–2707.

Skelton, R.J., Brady, B., Khoja, S., Sahoo, D., Engel, J., Arasaratnam, D., Saleh, K.K., Abilez, O.J., Zhao, P., Stanley, E.G., et al. (2016). CD13 and ROR2 permit isolation of highly enriched cardiac mesoderm from differentiating human embryonic stem cells. Stem Cell Rep. *6*, 95–108.

Srivastava, D., Cserjesi, P., and Olson, E.N. (1995). A subclass of bHLH proteins required for cardiac morphogenesis. Science *270*, 1995–1999.

Srivastava, D., Thomas, T., Lin, Q., Kirby, M.L., Brown, D., and Olson, E.N. (1997). Regulation of cardiac mesodermal and neural crest development by the bHLH transcription factor, dHAND. Nat. Genet. *16*, 154–160.

Takaki, T., Inagaki, A., Chonabayashi, K., Inoue, K., Miki, K., Ohno, S., Makiyama, T., Horie, M., and Yoshida, Y. (2020). Optical recording of action potentials in human induced pluripotent stem cell-derived cardiac single cells and monolayers generated from long QT syndrome type 1 patients (vol 2019, 7532657, 2019). Stem Cells Int. *2020*.

Takeuchi, T. (2014). Regulation of cardiomyocyte proliferation during development and regeneration. Dev. Growth Differ. *56*, 402–409.

Togi, K., Kawamoto, T., Yamauchi, R., Yoshida, Y., Kita, T., and Tanaka, M. (2004). Role of Hand1/eHAND in the dorso-ventral patterning and interventricular septum formation in the embryonic heart. Mol. Cell Biol. *24*, 4627–4635.

Tsankov, A.M., Gu, H., Akopian, V., Ziller, M.J., Donaghey, J., Amit, I., Gnirke, A., and Meissner, A. (2015). Transcription factor binding dynamics during human ES cell differentiation. Nature *518*, 344–349.

Tsuchihashi, T., Maeda, J., Shin, C.H., Ivey, K.N., Black, B.L., Olson, E.N., Yamagishi, H., and Srivastava, D. (2011). Hand2 function in second heart field progenitors is essential for cardiogenesis. Dev. Biol. *351*, 62–69.

Vincentz, J.W., Toolan, K.P., Zhang, W., and Firulli, A.B. (2017). Hand factor ablation causes defective left ventricular chamber development and compromised adult cardiac function. PLoS Genet. *13*, e1006922.

Woltjen, K., Michael, I.P., Mohseni, P., Desai, R., Mileikovsky, M., Hamalainen, R., Cowling, R., Wang, W., Liu, P., Gertsenstein, M., et al. (2009). piggyBac transposition reprograms fibroblasts to induced pluripotent stem cells. Nature *458*, 766–770.

Wu, S.M., Chien, K.R., and Mummery, C. (2008). Origins and fates of cardiovascular progenitor cells. Cell *132*, 537–543.

Yang, L., Soonpaa, M.H., Adler, E.D., Roepke, T.K., Kattman, S.J., Kennedy, M., Henckaerts, E., Bonham, K., Abbott, G.W., Linden, R.M., et al. (2008). Human cardiovascular progenitor cells develop from a KDR plus embryonic-stem-cell-derived population. Nature *453*, 524–U526.

Ye, B., Li, L., Xu, H., Chen, Y., and Li, F. (2019). Opposing roles of TCF7/LEF1 and TCF7L2 in cyclin D2 and Bmp4 expression and cardiomyocyte cell cycle control during late heart development. Lab. Invest. *99*, 807–818.

Zhang, J.Z., Termglinchan, V., Shao, N.Y., Itzhaki, I., Liu, C., Ma, N., Tian, L., Wang, V.Y., Chang, A.C.Y., Guo, H.C., et al. (2019). A human iPSC double-reporter system enables purification of cardiac lineage subpopulations with distinct function and drug response profiles. Cell Stem Cell *24*, 802.

Stem Cell Reports, Volume *16*

Supplemental Information

Expression dynamics of HAND1/2 in *in vitro* human cardiomyocyte differentiation

Chikako Okubo, Megumi Narita, Azusa Inagaki, Misato Nishikawa, Akitsu Hotta, Shinya Yamanaka, and Yoshinori Yoshida

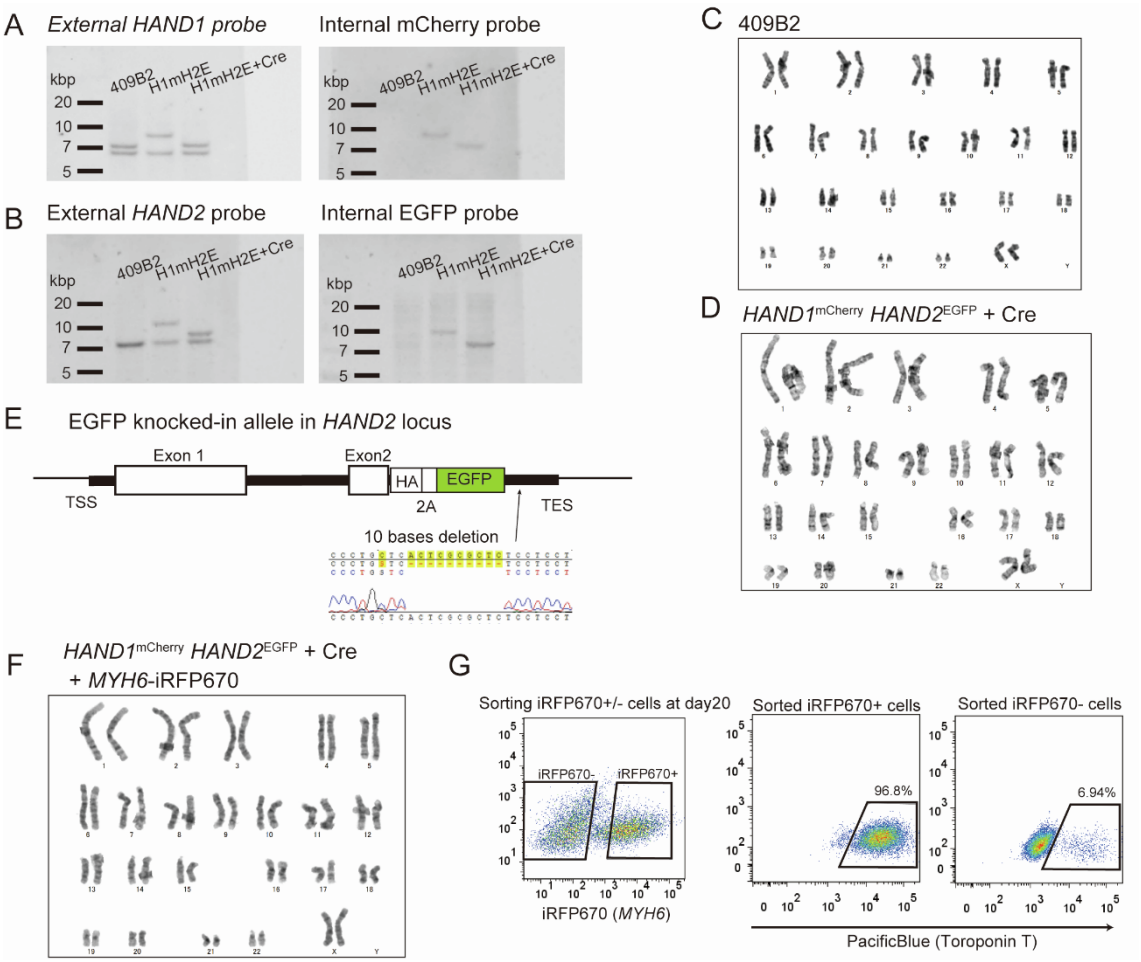

Figure S1. Construction of the *HAND1*^{mCherry}, *HAND2*^{EGFP} and *MYH6*-iRFP670 triple reporter line. Related to Figure 1.

(A and B) Southern blotting analyses of the parental hiPSC line (409B2), *HAND1*^{mCherry} *HAND2*^{EGFP} knocked-in double reporter line (H1mH2E) and Cre-treated double reporter line (H1mH2E+Cre) with external *HAND1* and *HAND2* probes and internal mCherry and EGFP probes, respectively. 409B2 showed two bands for the *HAND1* probe, suggesting a heterozygous mutation in the HindIII region.

(C and D) Karyotypes of parental 409B2 hiPSC and *HAND1*^{mCherry} *HAND2*^{EGFP} reporter lines after removal of the selection cassettes.

(E) A 10-base deletion was generated downstream of the *HAND2* coding region in the double reporter line. HA, HA-tag; 2A, 2A peptide; TSS, transcription start site; TES, transcription end site.

(F) Karyotype of the *HAND1*^{mCherry} *HAND2*^{EGFP} *MYH6*-iRFP670 triple reporter line.

(G) FACS plots show the expression of iRFP670 on day 20 (left) and expression of Troponin T in sorted iRFP670+ (middle) and iRFP670- populations (right).

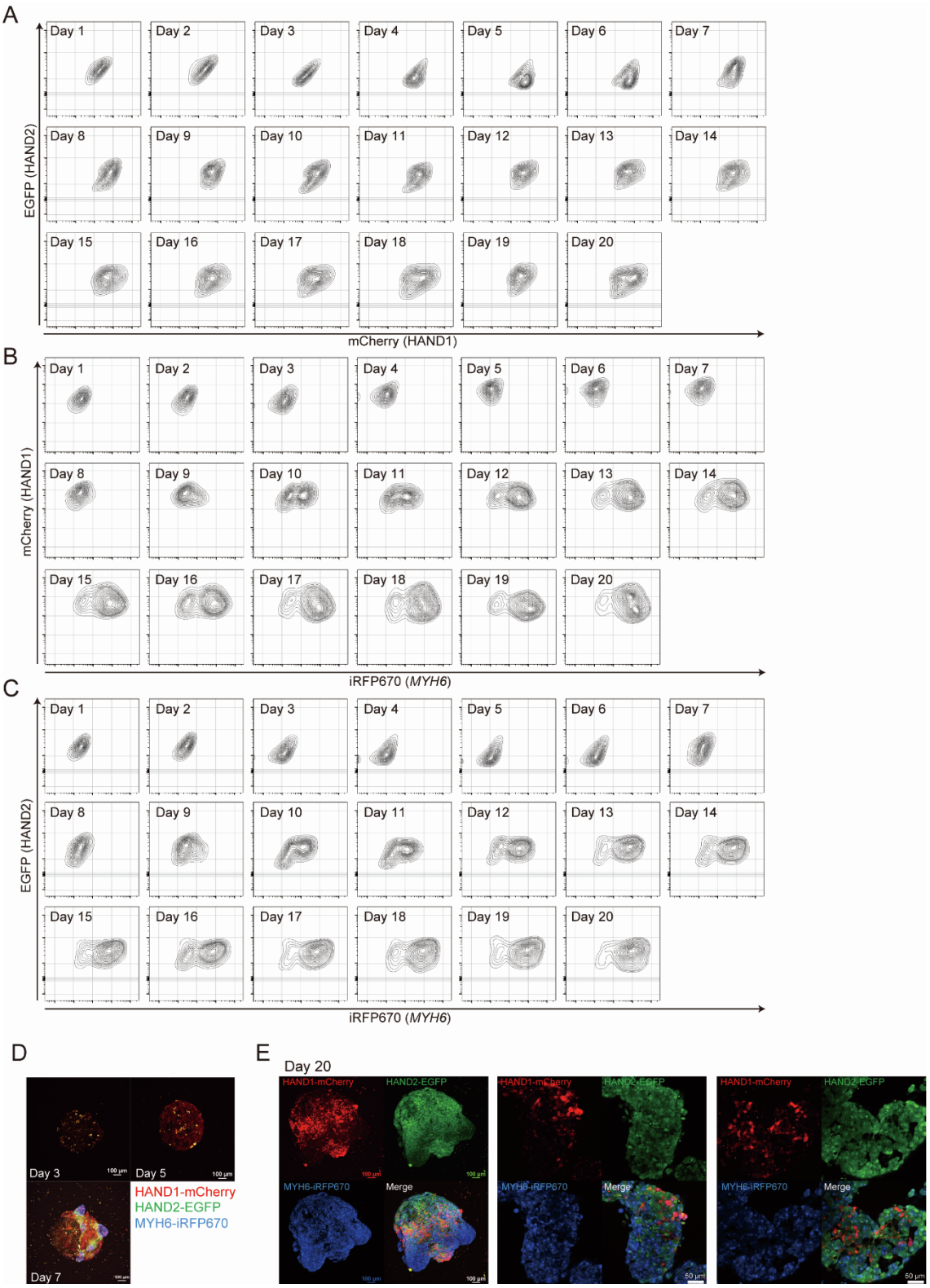

Figure S2. Flowcytometry analysis and confocal images of the *HAND1*^{mCherry} *HAND2*^{EGFP} *MYH6*-iRFP670 triple reporter line in the EB-based differentiation protocol. Related to Figure 1.

(A) Representative FACS plots of the expression dynamics of mCherry and EGFP from day 1 to day 20.
(B) Representative FACS plots of the expression dynamics of mCherry and iRFP670 from day 1 to day 20.
(C) Representative FACS plots of the expression dynamics of EGFP and iRFP670 from day 1 to day 20.
(D) Images of EBs on days 3, 5 and 7. Scale bars, 100 μm.
(E) Images of an EB on day 20 (left). Scale bar, 100 μm. Two sections of the EB (middle and right). Scale bars, 50 μm.

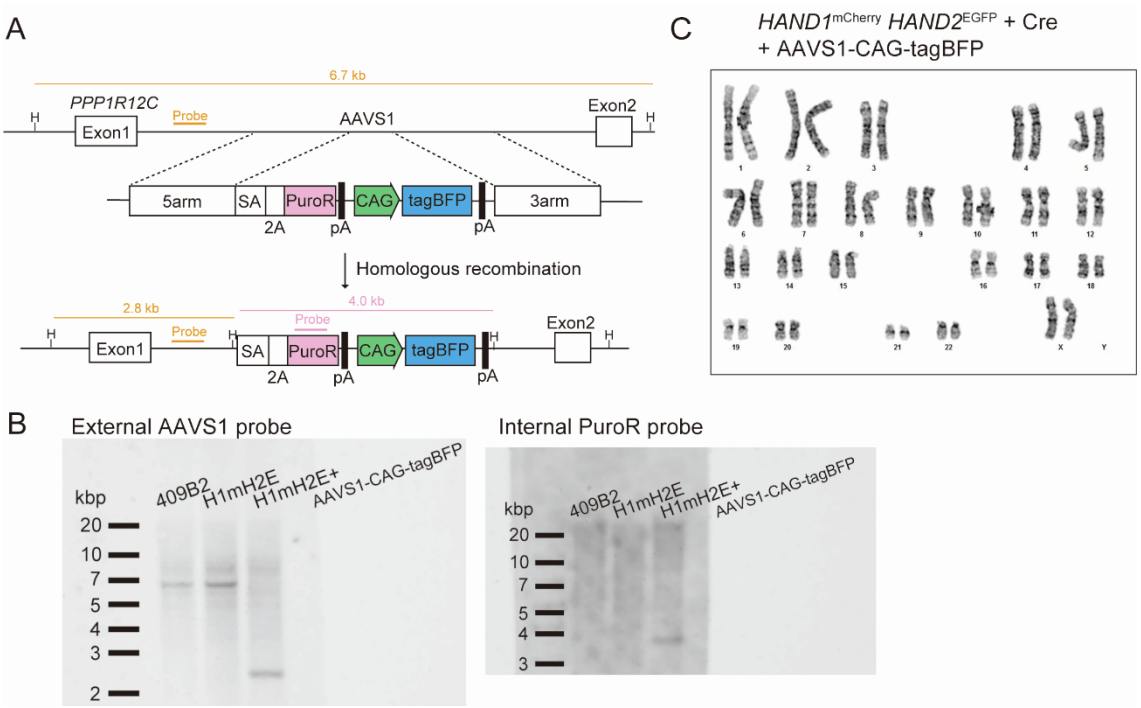

Figure S3. Construction of the AAVS1-CAG-tagBFP triple reporter line from the *HAND1*^{mCherry} *HAND2*^{EGFP} double reporter line. Related to Figure 2.

(A) Scheme of the tagBFP knock-in AAVS1 locus. SA, splicing acceptor; 2A, 2A peptide; PuroR, puromycin resistance genes; pA, poly adenosine sequence; CAG, CAG promoter sequence; 5arm, 5' homology arm; 3arm, 3' homology arm. HindIII (H) was used to digest genomic DNA for Southern blotting. Orange lines indicate external and internal probes for Southern blotting with expected band sizes.

(B) Southern blots of the external AAVS1 probe (left) and internal puromycin resistance gene probe (right).

(C) The *HAND1*^{mCherry}, *HAND2*^{EGFP} and AAVS1-CAG-tagBFP triple reporter line shows normal karyotype.

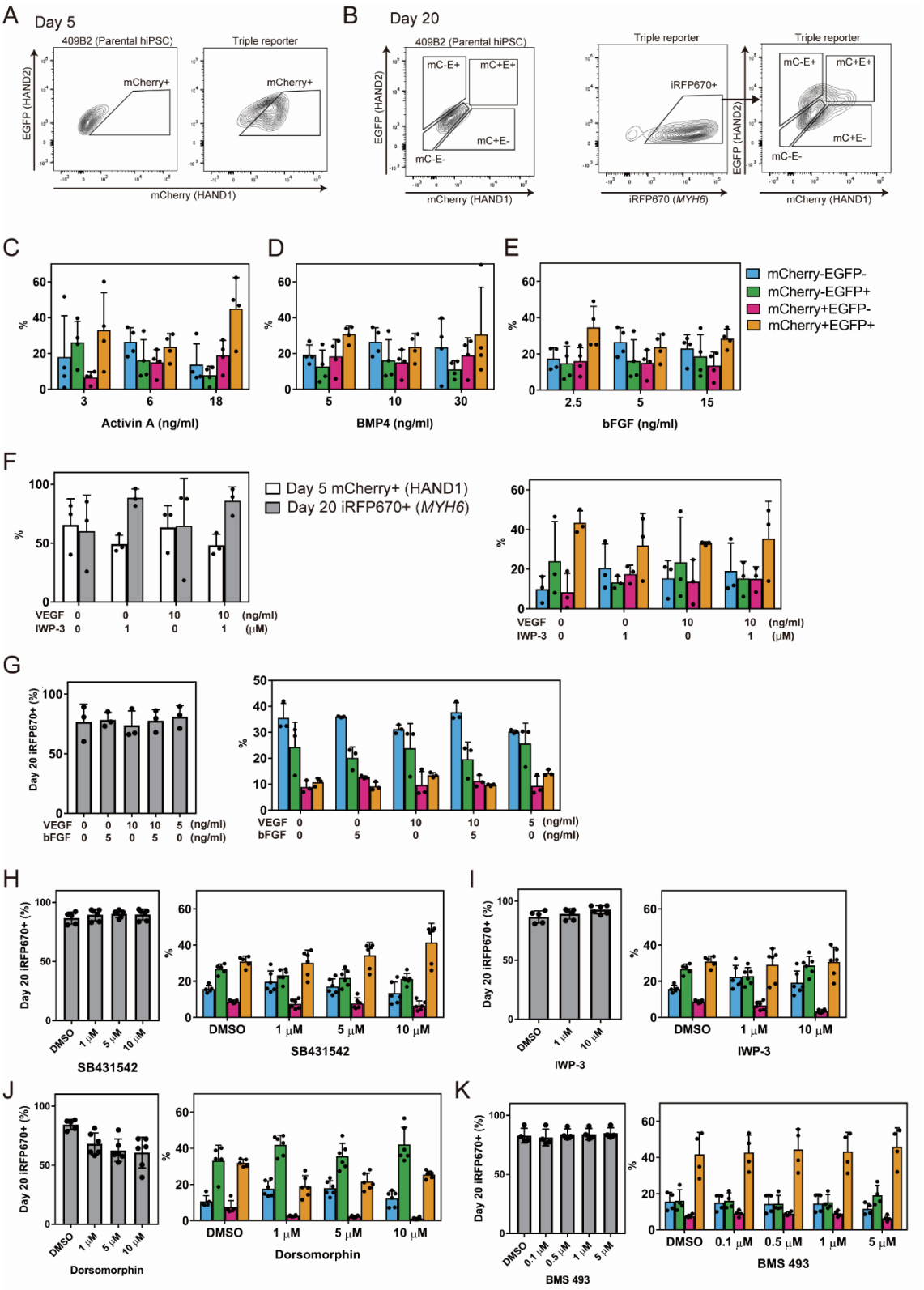

Figure S4. Effects of cytokines on *HAND1* and *HAND2* expression. Related to Figure 3.
(A) Representative FACS plots of mCherry expression in the parental hiPSC line (409B2) and triple reporter line on day 5.

(B) Representative FACS plots of iRFP670, mCherry (mC) and EGFP (E) expression in the triple reporter line and parental hiPSC line on day 20.
(C-E) Percentages of iRFP670+ CM subpopulations on day 20 with various concentrations of Activin A (C), BMP4 (D) and bFGF (E) in day 0-1 medium (n = 4 independent experiments). The ventricular protocol was used for the other stages.
(F) Percentages of mCherry+ cells on day 5, iRFP670+ cells on day 20 (left), and iRFP670+ CM subpopulations on day 20 (right) at different VEGF and IWP-3 quantities in day 3 medium (n = 3 independent experiments). The ventricular protocol was used for the other stages.
(G) Percentages of iRFP670+ CMs on day 20 (left) and iRFP670+ CM subpopulations on day 20 (right) with different quantities of VEGF and bFGF in day7-20 medium (n = 3 independent experiments). The ventricular protocol was used for the other stages.
(H-K) Percentages of iRFP670+ CMs on day 20 (left) and iRFP670+ CM subpopulations on day 20 (right) with the chemical inhibitors SB431542 (H), IWP-3 (I), Dorsomorphin (J), and BMS 493 (K) (n = 4-6 independent experiments). Data represent means ± SD.

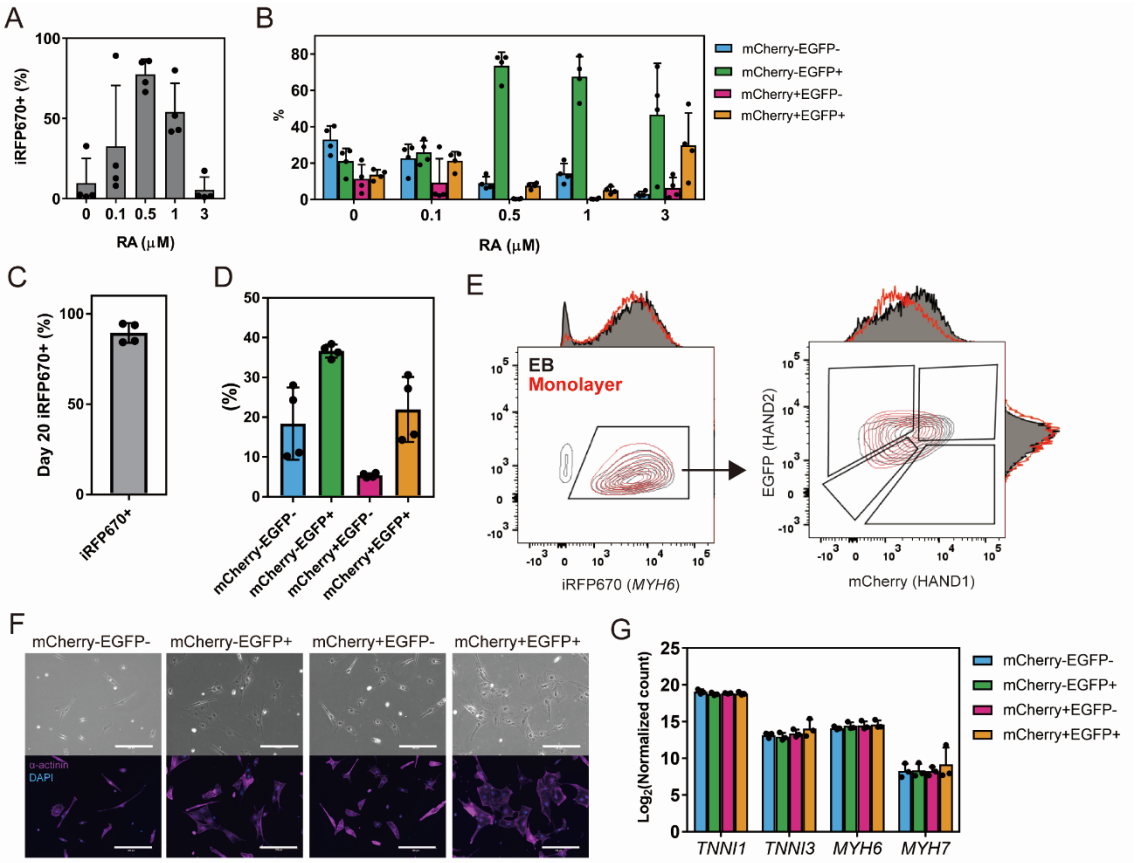

Figure S5. Distribution of CM subpopulations in the atrial differentiation and monolayer differentiation protocol and profiling of the subpopulations in ventricular differentiation protocol. Related to Figures 4 and 5.

(A) Frequency of iRFP670+ CMs on day 20 with the atrial protocol (n = 4 independent experiments). *p < 0.05, **p < 0.01 by one-way ANOVA with Dunnett's test comparing to 0 μM.

(B) Percentages of the iRFP670+ CM subpopulations shown in A.

(C) Frequency of iRFP670+ CMs on day 20 with the monolayer protocol (n = 4 independent experiments).

(D) Percentages of iRFP670+ CM subpopulations in C.

(E) Representative overlayed FACS plots of the expressions of iRFP670, mCherry and EGFP from the EB protocol and monolayer protocol.

(F) Immunohistochemistry with anti α-actinin antibody of each CM subpopulation. Scale bars, 200 μm.

(G) Expression levels of immature CM marker genes (MYH6 and TNNI1) and mature CM marker genes (MYH7 and TNNI3) from the RNA-seq data of ventricular CM subpopulations on day 20. Data represent means ± SD.

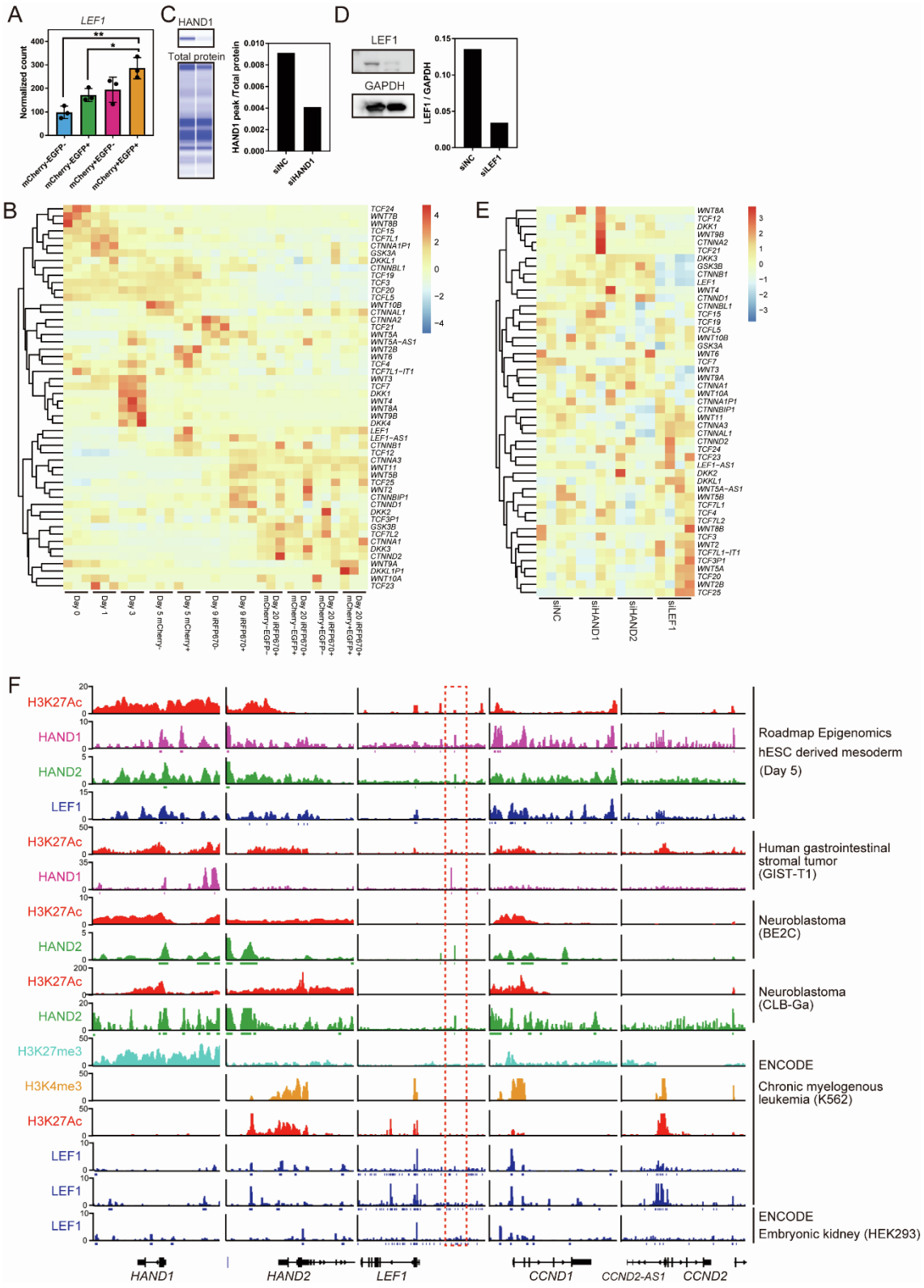

Figure S6. WNT signaling and knockdown of *HAND1*, *HAND2* and *LEF1*. Related to Figure 6.

(A) Normalized counts of *LEF1* from the RNA-seq data of ventricular iRFP670+ CM subpopulations. (n = 3 independent experiments). *p < 0.05, **p < 0.01 by one-way ANOVA with Tukey's multiple comparisons test. Data represent means ± SD.
(B) Heatmap and clustering of scaled expression levels of WNT signaling molecules. Days 0, 3, 5 (isolated mCherry- and mCherry+ populations), 9 (isolated iRFP670- and iRFP670+ populations) and 20 (isolated subpopulations in iRFP670+ CMs) were collected from the ventricular CM differentiation (n = 3 independent experiments).
(C) Knockdown efficiency of HAND1 by the Wes automated capillary electrophoresis system. The expression level of HAND1 protein was normalized with total protein.
(D) Knockdown efficiency of LEF1 by western blotting. The expression level of LEF1 protein was normalized with GAPDH.
(E) Heatmap and clustering of scaled expression levels of WNT signaling molecules in the knockdown of *HAND1*, *HAND2* and *LEF1* samples. The sorted CMs were transfected at day 15 with siRNAs for negative control (siNC), *HAND1* (siHAND1), *HAND2* (siHAND2) and *LEF1* (siLEF1), and the RNAs were collected on day 20 (n = 4 independent experiments).
(F) ChIP-seq tracks for H3K27Ac, H3K4me3, H3K27me3, HAND1, HAND2 and/or LEF1 at 5 loci (*HAND1*, *HAND2*, *LEF1*, *CCND1* and *CCND2*) in human ESC-derived mesodermal cells, human cancer cell lines (GIST-T1, BE2C, CLB-Ga, K562) and the HEK293 cell line. The dashed red rectangle highlights the binding sites of HAND1 and HAND2 upstream of *LEF1*.

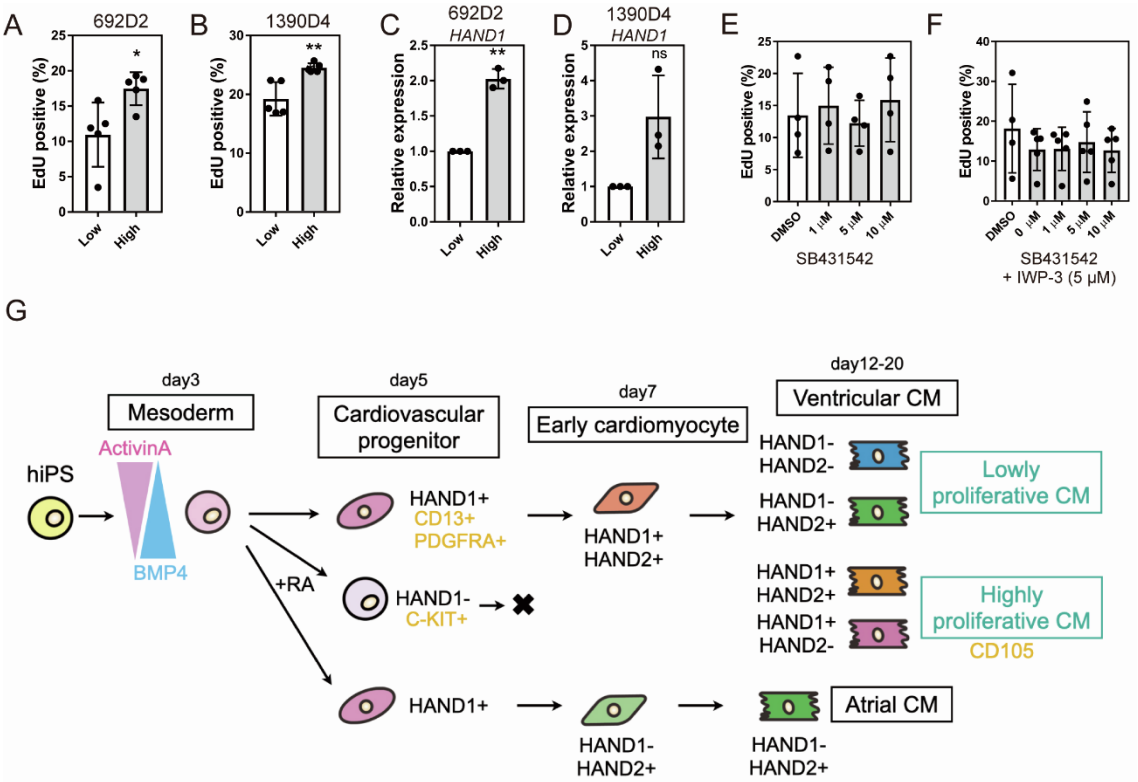

Figure S7. The utility of CD105 as a proliferative cardiomyocyte marker and schematic diagram of the expression patterns of *HAND1* and *HAND2* for cardiac *in vitro* differentiation. Related to Figure 7.

(A and B) Percentages of EdU+ cells on day 23 in lineage (CD90, CD31, CD49a, CD140b)-negative and SIRPA-positive CMs and CD105-APC-high or -low CMs isolated on day 20 from 692D2 (A) and 1390D4 (B) (n = 5 independent experiments). *p < 0.05, **p < 0.01 by unpaired t-test.

(C and D) Expression level of *HAND1* in CD105-high and -low CMs isolated on day 20 of 692D2 (C) and 1390D4 (D) (n = 3 independent experiments). **p < 0.01 by Welch's t-test.

(E) EdU+ ratio with TGFβ signal inhibitor (SB431542) treatment (n = 4 independent experiments). All comparisons were not significant by one-way ANOVA with Dunnett's multiple comparisons test (compared to DMSO).

(F) EdU+ ratio with the administration of SB and 5 μM IWP-3 (n = 5 independent experiments). All comparisons were not significant by one-way ANOVA with Dunnett's multiple comparisons test (compared to DMSO). Data represent means ± SD.

(G) Schematic representation of the differential stages *in vitro* based on the expressions of *HAND1* and *HAND2* and surface markers.

Table S1. RNA-seq data of genes for each of the 4 subpopulations in day 20 iRFP670+ CMs from the ventricular protocol. Related to Figure 5. Please see associated excel file (TableS1.xlsx).

Table S2. Results of the gene set enrichment analysis of the Reactome pathway using genes in cluster 3. Significantly enriched pathways are listed (adjustment p-value < 0.05). Related to Figure 5. Please see the associated excel file (TableS2.xlsx).

Table S3. List of ChIP-seq data. Related to Figure S6.

Target	Cell type	Accessions number	PMID (Reference)
H3K27Ac	hESC derived mesoderm (Day 5)	GSM1505669	25693565 (Tsankov et al., 2015)
HAND1	hESC derived mesoderm (Day 5)	GSM1505812	25693565 (Tsankov et al., 2015)
HAND2	hESC derived mesoderm (Day 5)	GSM1505811	25693565 (Tsankov et al., 2015)
LEF1	hESC derived mesoderm (Day 5)	GSM1505691	25693565 (Tsankov et al., 2015)
H3K27Ac	GIST-T1	GSM2527250	29866822 (Hemming et al., 2018)
HAND1	GIST-T1	GSM2527318	29866822 (Hemming et al., 2018)
H3K27Ac	BE2C	GSM3128275	30127528 (Durbin et al., 2018)
HAND2	BE2C	GSM2486155	30127528 (Durbin et al., 2018)
H3K27Ac	CLB-GA	GSM2664317	28740262 (Boeva et al., 2017)
HAND2	CLB-GA	GSM2664371	28740262 (Boeva et al., 2017)
H3K27me3	K562	GSM788088	22955616 (Consortium, 2012)
H3K4me3	K562	GSE96303	22955616 (Consortium, 2012)
H3K27Ac	K562	GSM733656	22955616 (Consortium, 2012)
LEF1	HEK293T	GSE105382	22955616 (Consortium, 2012)
LEF1	K562	GSE105908	22955616 (Consortium, 2012)
LEF1	K562	GSE91682	22955616 (Consortium, 2012)

Table S4. List of DNA oligos/primers and vectors. Related to Figures 1, 2, S1 and S3.
Please see the associated excel file (TableS4.xlsx).

Table S5. List of antibodies. Related to Figures 2, 7, S1, S5, and S7.

Name	Vendor	Catalog #	Dilution
Anti-Troponin T	Thermo Scientific	#MS-295-P	1:500
Anti-Mouse Pacific Blue	Invitrogen	P31581	1:200
Anti-human CD13	BioLegend	301715	1:50
Anti-human CD140a (PDGFRA)	BD	562799	1:50
Anti-Human CD117 (C-KIT)	BD	562435	1:50
BV421 mouse IgG1γ	BioLegend	400158	1:50
Anti-α-Actinin	SIGMA	A7811	1:800
Anti-Mouse Alexa Fluor 546	Invitrogen	A11030	1:400
Anti-CD105	Miltenyi Biotec	130-099-125	1:50
Anti-CD140b	BD	558821	1:50
Anti-CD31	BD	555446	1:50
Anti-CD49a	BD	559596	1:50
Anti-CD90	BD	555596	1:50

Anti-CD172a/b (SIRPA)	BioLegend	323808	1:50

Table S6. List of probes used in TaqMan Gene Expression Assays. Related to Figures 2, 4 and 6.

Target gene name	ID
ACTB	Hs00357333_g1
GAPDH	Hs99999905_m1
NKX2-5	HS00231763_m1
TBX5	Hs00361155_m1
ISL1	Hs01099686_m1
TBX20	Hs00396596_m1
FGF8	Hs00171832_m1
FGF10	Hs00610298_m1
ISL1	Hs01099686_m1
HCN4	Hs00975492_m1
NR2F2	Hs00819630_m1
HAND1	Hs02330376_s1
HAND2	Hs00232769_m1
LEF1	Hs01547250_m1

Table S7. List of siRNAs. Related to Figure 6.

Name	ID
Silencer™ Select Pre-Designed siRNA HAND1	s18035
Silencer™ Select Pre-Designed siRNA HAND1	s18037
Silencer™ Select Pre-Designed siRNA HAND2	s225137
Silencer™ Select Pre-Designed siRNA HAND2	s18131
Silencer™ Select Pre-Designed siRNA HAND2	s18132
Silencer™ Select Pre-Designed siRNA LEF1	s27616
Silencer™ Select Negative Control No. 1 siRNA	4390843
Silencer™ Select Negative Control No. 2 siRNA	4390846

Supplemental Experimental Procedures

Establishment of *HAND1*^{mCherry} and *HAND2*^{EGFP} double reporter line

Using the CRISPR-Cas9 system, two guide RNAs (gRNAs) were designed close to the stop codons of *HAND1* and *HAND2* genes, respectively, and cloned into pHL-H1-ccdB-mEF1a-RiH plasmid (Li et al., 2015). We constructed two targeting vectors, a FLAG-2A-mCherry (floxed PGK-Puromycin resistance) donor plasmid containing homology to the 3' of the *HAND1* gene locus and a HA-2A-EGFP (floxed-PGK-Neomycin resistance) donor plasmid containing homology to the 3' end of the *HAND2* gene locus. For homologous recombination, the homology arms were cloned 1000 bases up- and downstream of the *HAND1* and *HAND2* stop codons. For the knock-in experiments, we used 409B2 hiPSCs, which were established by the episomal method and cultured on neomycin and puromycin resistance SNL feeder cells (Okita et al., 2011). Electroporation was done with a NEPA 21 (NEPAGENE) following a previously described method with modifications (Li et al., 2015). Briefly, 5×10^5 hiPSCs were transfected with 2.5 μg Cas9 vector (pHL-EF1a-SphcCas9-iP-A), 3 μg of each targeting vector and 2.5 μg of each gRNA vector simultaneously. After 48 hours, 0.5 μg/ml puromycin (Sigma-Aldrich) was administered for 5 days, and subsequently 50 μg/ml G418 (Gibco) was administered until subcloning. The cloned hiPSCs were genotyped by PCR and sequenced at the junction of the homologous arms. Apart from a 10-base deletion downstream of the *HAND2* homology arm, both reporter cassettes were successfully inserted at the target sites. In addition, we performed Southern blotting to choose the hiPSC line with heterozygous knock-in for both *HAND1* and *HAND2* reporter cassettes. All DNA oligos/primers and vectors are listed in Table S4.

Removing the selection cassettes with Cre

To remove the selection cassettes, the hiPSCs were transiently transfected with a Cre-expressing vector (1 μg/ml pCAG-Cre-Blast, kindly provided by Dr. Keisuke Okita) using FuGENE HD (Promega) following the manufacturer's instruction (Table S4). After plating the hiPSCs on dishes coated with 10 μg/ml Matrigel (Corning), the cells were cultured in mouse embryonic fibroblast (MEF)-conditioned medium with 10 μg/ml Blasticidin S (Funakoshi) for 2 days. Blasticidin-resistant subclones were established, and removal of the puromycin and neomycin resistance cassettes was confirmed by PCR, sequencing and Southern

blotting.

Establishment of AAVS1-CAG-tagBFP, *HAND1*^{mCherry} and *HAND2*^{EGFP} triple reporter line
For the constitutive expression of tagBFP, its coding sequence was knocked into the AAVS1 locus, which allowed for the stable expression of the CAG promoter to drive the transgene during differentiation, of double reporter hiPSCs using TALEN (Oceguera-Yanez et al., 2016). The targeting vector has a splicing acceptor with the puromycin resistance gene connected to CAG-tagBFP-pA, which was originated from AAVS1-CAG-hrGFP (a gift from Dr. Su-Chun Zhang (Addgene plasmid #52344)) (Qian et al., 2014). 2.5 μg of each targeting vector and the TALEN left- and right-arm vectors hAAVS1 1L TALEN and hAAVS1 1R TALEN (gifts from Feng Zhang (Addgene plasmid #35431 and #35432)) were transfected by electroporation as explained above for the CRISPR-Cas9 knock-in (Sanjana et al., 2012). Two days after the electroporation, tagBFP+ cells were sorted and subcloned. The subclones were confirmed by sequencing, karyotyping and Southern blotting. All DNA oligos/primers and vectors used are listed in Table S4.

Establishment of *MYH6* reporter line
The *MYH6*-iRFP670 *piggyBac* vector was transfected into the double reporter iPSCs described above. We confirmed normal karyotype by G-banding analysis. Cells undergoing CM differentiation, i.e., iRFP670+ cells, were 96.8% positive for Troponin T (Thermo Scientific, #MS-295-P), whereas iRFP670- cells were only 6.9% positive for Troponin T, confirming the functionality of the *MYH6* CM reporter. All antibodies used are listed in Table S5.

Fluorescence activated cell sorting (FACS) and immunostaining
For FACS, EBs were dissociated with Accumax (Innovative Cell Technologies) for 15 minutes at 37°C. EBs past day 7 were treated with collagenase type I (Sigma-Aldrich) for 4-12 hours before the dissociation. All samples for the FACS were suspended with FACS buffer (5% FBS-PBS) including 0.5 μg/ml DAPI (Thermo Scientific) and 10 μg/ml DNase (CALBIOCHEM). DAPI+ cells were eliminated from the analysis. For reporter cells, 409B2, the parent hiPSC line of the reporter cells, was used as a negative control. For the flowcytometric analysis of day 5 EBs, the dissociated cells were stained with antibodies against human CD13-BV421, PDGFRA-BV421 and C-KIT-BV421 on ice for 30 minutes. For day 20, the cells were stained with CD105-APC antibody on ice for 30 minutes. For CMs derived from non-reporter hiPSCs, the dissociated cells were stained with CD105-APC, lineage markers-PE (CD140b, CD31, CD49a, CD90) and SIRPA-PE/Cy7 (CD170a/b) antibodies on ice for 30 minutes. All antibodies used are listed in Table S5.

Monolayer differentiation of cardiomyocytes
For the first 5 days, hiPSCs were differentiated to CMs following the EB method. On day 5, the cells were dissociated and seeded into a 24-well plate coated with fibronectin (Sigma-Aldrich) (50×10^4 cells/well) in maintenance medium including 5 ng/ml VEGF. The maintenance medium was refreshed every 2-3 days.

Mixed co-culture of tagBFP triple reporter line
To trace mCherry- cells, day 5 EBs were dissociated into single cells using Accumax for 5 minutes at 37°C, and tagBFP+ cells were sorted as mCherry- or mCherry+ (Figure 2C). Then, the tagBFP-labeled cells (0.8×10^4 cells/well) and non-labeled cells (7.2×10^4 cells/well), which were derived from the parental double reporter line, were re-aggregated to a total of 8×10^3 cells/well with 0.5% Matrigel.

Microscopy and immunostaining
The sorted cells were seeded on 24-well plates coated with fibronectin. After 4 days, the cells were fixed with 4% paraformaldehyde (Nacalai) for 30 minutes at room temperature and permeabilized with 0.5% saponin (Sigma-Aldrich). Cells stained with mouse anti-actin (1:800, Sigma-Aldrich, A7811), goat anti-mouse Alexa Fluor 546 (1:400, Invitrogen, A11030) and 1 μg/ml Hoechst 33342 (Invitrogen) were detected using a fluorescence microscope (KEYENCE BZ-X700) (Table S5).

Confocal imaging
For confocal imaging, the EBs were put on a glass-bottom 96-well plate (Corning) in FACS buffer with 10 μM Y-27632 to stop the beating. The expressions of mCherry, EGFP and iRFP670 in live cells were detected using a confocal microscope (A1R MP+, Nikon).

Southern blotting
Using cell lysis solution (QIAGEN), the genome DNA of the iPSCs was purified using a DNeasy Blood and Tissue Kit (QIAGEN). Genome DNA (3 μg) was digested using HindIII (New England Biolabs) overnight, separated on a 0.8% agarose gel, and transferred to a nylon membrane (GE health care). The membrane was incubated at 42℃ overnight with a digozigenin (DIG)-labeled DNA probe in DIG Easy Hyb buffer (Roche Life Science). After washing, the membrane was incubated in skim milk with alkaline phosphatase-conjugated anti-DIG antibody (1:10000, Anti-Digoxigenin-AP, Fab fragments, Roche Life Science). The signals were detected using CDP-*Star*® reagent (Roche Life Science) and a LAS3000 imaging system (FUJI FILM). The two probes were designed in the internal and external regions of the knock-in sequences generated by the PCR using the primer sets described in Table S4.

RNA sequencing and data analysis
Total RNAs were extracted using the miRNeasy Micro Kit and purified by RNase-Free DNase Set (QIAGEN) according to the manufacturer's protocols. Libraries were generated using 100 μg RNA and TruSeq Stranded total RNA with the Ribo-Zero Gold LT Sample Prep Kit, Set A and B (Illumina) according to the manufacturer's instruction. The NextSeq 500/550 High Output Kit v2 (75 Cycles) (Illumina) was used for sequencing. After trimming adapter sequences using cutadapt-1.15 (Martin, 2011), we removed the reads mapped to ribosomal RNA using samtools and bowtie2 (Langmead and Salzberg, 2012; Li et al., 2009). The reads mapped to the human genome (GRCh38 from the UCSC Genome Browser) using STAR (version 2.5.4a), underwent a quality check using RSeQC (version 2.6.4) (Dobin et al., 2013; Wang et al., 2012). The reads were counted using HTSeq (version 0.9.1) with the GENCODE annotation file (version 27) (Anders et al., 2014; Frankish et al., 2019). The counts were normalized using DESeq2 (version 1.24.0) in R (version 3.6.1) (Love et al., 2014). Using the DESeq2 package, PCA and likelihood ratio tests were performed. Gene clustering was performed using DEGreport (version 1.20.0) packages (Pantano, 2017). ClusterProfiler (version 3.12.0) and ReactomePA (version 1.28.0) were used for GO and pathway enrichment analysis, respectively (Yu and He, 2016; Yu et al., 2012). All heatmaps were produced using the pheatmap package. For upstream analysis, we used the geneXplain platform and the genes of cluster 2. We performed "Upstream analysis Transfac and Geneways" with default settings (Kel et al., 2006; Koschmann et al., 2015).

EdU assay
Sorted CMs were seeded on fibronectin-coated plates (5-6 × 10^5 cells/well in a 6-well plate or 1.0-1.5 × 10^5 cells/well in a 12-well plate). After 2 days for recovery, the cells were treated with 1 μM EdU for 18 hours using the Click-iT® EdU Flow Cytometry Assay Kit (Invitrogen) following the manufacturer's instructions.

Evaluation of knockdown levels
Five days after the transfection of siRNA into purified CMs, the CMs were washed with PBS two times and then resuspended in M-PER (Thermo) containing Protease inhibitor cocktail (1:100, Nacalai). Protein concentrations were determined using the BAC assay (Bio Lad). To detect the knockdown efficiency of HAND1 by siRNA transfection, the 12-230 kDa Separation Module (Protein Simple) and Wes automated capillary electrophoresis system (Protein Simple) were used.

Anti-HAND1 (1:20, AF3168, R&D Systems) was used as the primary antibody, and HRP-conjugated secondary antibodies were also used. Protein loading was normalized using the Total Protein Detection Module (Protein Simple). The data were analyzed and visualized using Compass (Protein Simple). For LEF1, conventional western blotting was performed. In brief, the proteins were separated in 10-20% gel (FUJIFILM) with 10x Tris/Glycine/SDS Buffer (BIOLAD) and transferred to a nitrocellulose membrane (Merck Millipore) with 10x Tris/Glycine Buffer (BIOLAD). The membrane was blocked with 5% skim milk (FUJIFILM) for 60 min at room temperature with constant agitation and then incubated with primary anti-LEF1 (1:1000, A303-486A, BETHYL) at 4 ℃ overnight. The membrane was washed three times with Tris-buffered saline. Then, the membrane was incubated with secondary antibody (1:5000, goat anti-rabbit IgG-HRP, sc-2004, Santa Cruz Biotechnology) diluted in Bullet Blocking One for Western Blotting (Nacalai tesque) for 1 hour at room temperature. After the secondary antibody reaction, the membrane was incubated in chemiluminescent HRP substrate for 5 min. Images were obtained using an ImageQuant LAS 4000 (Cytiva).

Chromatin Immunoprecipitation (ChIP) data analysis

All ChIP-seq data (wig and bed files) of HAND1, HAND2, LEF1, H3K27Ac, H3K4me3 and H3K27me3 immunoprecipitated samples mapped to hg19 were obtained from Gene Expression Omnibus (GEO) by NCBI and visualized by Integrative Genomics Viewer (Robinson et al., 2011) . The files are listed in Table S3.

Chemical inhibition and activation of signaling

To inhibit and activate WNT signaling, IWP-3 and CHIR99021 (FUJIFILM), respectively, were added to the maintenance medium from day 16 to day 18. For the knockdown experiments, these compounds were administered from day 17 to day 19. To investigate the effect of the CM sub-population distribution, IWP-3, SB, Dorsomorphin, and BSM 492 were administered from day 7 to day 20.

Supplemental References

Anders, S., Pyl, P.T., and Huber, W. (2014). HTSeq—a Python framework to work with high-throughput sequencing data. Bioinformatics *31*, 166-169.

Boeva, V., Louis-Brennetot, C., Peltier, A., Durand, S., Pierre-Eugene, C., Raynal, V., Etchevers, H.C., Thomas, S., Lermine, A., Daudigeos-Dubus, E.*, et al.* (2017). Heterogeneity of neuroblastoma cell identity defined by transcriptional circuitries. Nat Genet *49*, 1408-1413.

Consortium, E.P. (2012). An integrated encyclopedia of DNA elements in the human genome. Nature *489*, 57-74.

Dobin, A., Davis, C.A., Schlesinger, F., Drenkow, J., Zaleski, C., Jha, S., Batut, P., Chaisson, M., and Gingeras, T.R. (2013). STAR: ultrafast universal RNA-seq aligner. Bioinformatics *29*, 15-21.

Durbin, A.D., Zimmerman, M.W., Dharia, N.V., Abraham, B.J., Iniguez, A.B., Weichert-Leahey, N., He, S., Krill-Burger, J.M., Root, D.E., Vazquez, F.*, et al.* (2018). Selective gene dependencies in MYCN-amplified neuroblastoma include the core transcriptional regulatory circuitry. Nat Genet *50*, 1240-1246.

Frankish, A., Diekhans, M., Ferreira, A.M., Johnson, R., Jungreis, I., Loveland, J., Mudge, J.M., Sisu, C., Wright, J., Armstrong, J.*, et al.* (2019). GENCODE reference annotation for the human and mouse genomes. Nucleic Acids Res *47*, D766-D773.

Hemming, M.L., Lawlor, M.A., Zeid, R., Lesluyes, T., Fletcher, J.A., Raut, C.P., Sicinska, E.T., Chibon, F., Armstrong, S.A., Demetri, G.D.*, et al.* (2018). Gastrointestinal stromal tumor enhancers support a transcription factor network predictive of clinical outcome. Proc Natl Acad Sci U S A *115*, E5746-E5755.

Langmead, B., and Salzberg, S.L. (2012). Fast gapped-read alignment with Bowtie 2. Nat Methods *9*, 357-359.

Li, H., Handsaker, B., Wysoker, A., Fennell, T., Ruan, J., Homer, N., Marth, G., Abecasis, G., Durbin, R., and Genome Project Data Processing, S. (2009). The Sequence Alignment/Map format and SAMtools. Bioinformatics *25*, 2078-2079.

Love, M.I., Huber, W., and Anders, S. (2014). Moderated estimation of fold change and dispersion for RNA-seq data with DESeq2. Genome Biol *15*, 550.

Martin, M. (2011). Cutadapt removes adapter sequences from high-throughput sequencing reads. EMBnetjournal *17*, 10.

Pantano, L. (2017). DEGreport: Report of DEG analysis.

Robinson, J.T., Thorvaldsdottir, H., Winckler, W., Guttman, M., Lander, E.S., Getz, G., and Mesirov, J.P. (2011). Integrative genomics viewer. Nat Biotechnol *29*, 24-26.

Tsankov, A.M., Gu, H., Akopian, V., Ziller, M.J., Donaghey, J., Amit, I., Gnirke, A., and Meissner, A. (2015). Transcription factor binding dynamics during human ES cell differentiation. Nature *518*, 344-349.

Wang, L., Wang, S., and Li, W. (2012). RSeQC: quality control of RNA-seq experiments. Bioinformatics *28*, 2184-2185.

Yu, G., and He, Q.Y. (2016). ReactomePA: an R/Bioconductor package for reactome pathway analysis and visualization. Mol Biosyst *12*, 477-479.

Yu, G., Wang, L.G., Han, Y., and He, Q.Y. (2012). clusterProfiler: an R package for comparing

biological themes among gene clusters. OMICS *16*, 284-287.